# Cold polar molecules in two-dimensional traps: Tailoring interactions with external fields for novel quantum phases

A. Micheli,* G. Pupillo, H. P. Büchler, and P. Zoller
*Institute for Theoretical Physics, University of Innsbruck, A-6020 Innsbruck, Austria*
*and Institute for Quantum Optics and Quantum Information of the Austrian Academy of Sciences, A-6020, Innsbruck, Austria*
(Received 4 June 2007; published 3 October 2007)

We discuss techniques to engineer effective long-range interactions between polar molecules using external static electric and microwave fields. We consider a setup where molecules are trapped in a two-dimensional pancake geometry by a far-off-resonance optical trap, which ensures the stability of the dipolar collisions. We detail how to modify the *shape* and the strength of the long-range part of interaction potentials, which can be utilized to realize interesting quantum phases in the context of cold molecular gases.

DOI: 10.1103/PhysRevA.76.043604 PACS number(s): 03.75.Nt, 34.50.Rk, 33.80.−b

## I. INTRODUCTION

The realization of Bose-Einstein condensates (BECs) and quantum degenerate Fermi gases with cold atoms has been one of the highlights of experimental atomic physics during the last decade [1], and in view of recent progress in preparing cold molecules we expect a similarly spectacular development for molecular ensembles in the coming years [2–22]. The outstanding features of the physics of cold atomic and molecular gases are the microscopic knowledge of the many-body Hamiltonians, as realized in the experiments, combined with the possibility to control and tune system parameters via external fields. Examples are the trapping of atoms and molecules with magnetic, electric, and optical traps, allowing for the formation of quantum gases in one- (1D), two- (2D), and three-dimensional (3D) geometries, and the tuning of contact interparticle interactions by varying the scattering length via Feshbach resonances [23,24]. This control is the key for the experimental realization of fundamental quantum phases, as illustrated by the superfluid–Mott-insulator quantum phase transition with bosonic atoms in an optical lattice [25], and the BEC-BCS crossover in atomic Fermi gases [26–30].

As discussed in our recent work [31], polar molecules prepared in the electronic and vibrational ground state offer new possibilities to control interparticle interactions. In fact, effective interactions with a *given potential shape* can be engineered under conditions of tight 2D confinement, by applying static (dc) and microwave (ac) fields. The engineered potentials can display both repulsive and/or attractive character. This control of the interactions—in combination with low-dimensional trapping—opens the way to realizing novel quantum phases and quantum phase transitions. As an example, Ref. [31] discusses a quantum phase transition from a superfluid to a self-assembled crystal for a gas of polar molecules in the *strongly interacting limit*, where the stability of the collision processes is guaranteed by the confinement in a 2D geometry. It is the purpose of the present paper to present in some detail the molecular aspects behind this engineering of effective two-body interactions.

The interaction potential between atoms, in particular alkali-metal atoms in their electronic ground state, is dominated at large distances by an *attractive* $C_6/r^6$ potential. In the many-body Hamiltonian for a dilute quantum gas, this gives rise to an effective two-body short-range interaction in the form of a contact interaction with a scattering length $a_s$. Polar molecules have strong permanent electric dipole moments in their electronic-vibrational ground-state manifold, and pairs of molecules aligned by external dc or ac electric fields will interact via (comparatively strong) dipole-dipole interactions with characteristic long-range $1/r^3$ dependence [2,32–35]. These dipole-dipole interactions will be attractive or repulsive, depending on the relative orientation of the dipoles.

The alignment of the dipoles corresponds to the dressing of the lowest energy excitations of the internal molecular degrees of freedom, which are related to rotations of the molecule. The rotational dynamics can be manipulated using external electric dc and ac (microwave) fields. This dressing of rotational states by external fields together with the dipole-dipole interaction forms the basis to shape the effective molecular interactions.

One example discussed in Ref. [31] deals with polar molecules confined in a 2D (pancake) trap (see Fig. 1). The molecular dipoles are aligned perpendicular to the plane by a dc field. Thus, the effective 2D interactions are *repulsive* and *long range*, $V_{\mathrm{eff}}^{\mathrm{2D}}(\boldsymbol{\rho})=C_3/\rho^3$, with $\boldsymbol{\rho}=r\sin\vartheta(\cos\varphi,\sin\varphi)$ the 2D coordinate in the plane $z=0$ and $\rho=r\sin\vartheta$ (see Fig. 2, solid line). The interaction strength $C_3$ is proportional to the square of the induced dipole moment for the dressed rotational ground state. Depending on the interaction strength, we find the appearance of a crystalline phase, and an associated quantum melting to a superfluid phase as a function of the square of the induced dipole moment. The corresponding phase diagram is discussed in Ref. [31], and it is reproduced in Fig. 3 (see also Ref. [36]).

In the present work we present in detail the microscopic molecular theory underlying this engineering of the interaction potential for trapped polar molecules offered by dc and ac microwave fields. We focus both on potentials that are repulsive $1/r^3$ (dc field) and on potentials that have a marked "steplike" character, that is, the character of the repulsive potentials varies considerably in a small region of space (an ac plus a dc field). Three example cases of effective 2D potentials $V_{\mathrm{eff}}^{\mathrm{2D}}(\boldsymbol{\rho})$ are shown in Fig. 2. The use of multichro-

*andrea.micheli@uibk.ac.at

 

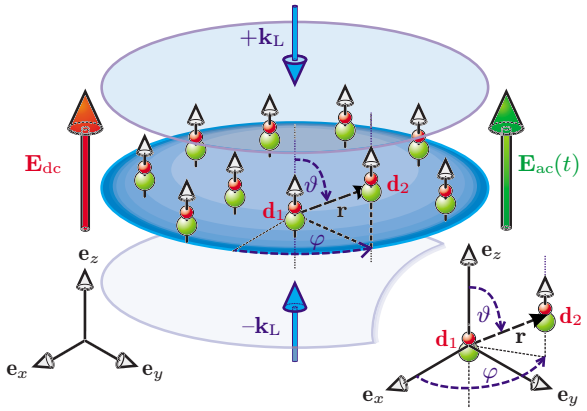


FIG. 1. (Color online) System setup: Polar molecules are trapped in the $(x,y)$ plane by an optical lattice made of two counterpropagating laser beams with wave vectors $\pm\mathbf{k}_L=\pm k_L\mathbf{e}_z$ (arrows on the top and bottom). The dipoles $\mathbf{d}_j$ are aligned in the $z$ direction by a dc electric field $\mathbf{E}_{dc}\equiv E_{dc}\mathbf{e}_z$ (arrow on the left). An ac (microwave) field $\mathbf{E}_{ac}$ is indicated (arrow on the right). Inset: Definition of polar ($\vartheta$) and azimuthal ($\varphi$) angles for the relative orientation of the intermolecular collision axis $\mathbf{r}$ with respect to a space-fixed frame with axes $\{\mathbf{e}_x,\mathbf{e}_y,\mathbf{e}_z\}$.

matic ac fields can lead to the realization of interesting potentials (for example, the attractive potential of Fig. 2); however, in this work we focus on monochromatic ac fields only.

In all cases, the derivation of the effective 2D interactions proceeds in two steps: First, we derive a set of Born-Oppenheimer (BO) potentials by diagonalizing the Hamiltonian for the relative motion of two particles for fixed molecular positions. Within an adiabatic approximation, the corresponding eigenvalues play the role of an effective 3D interaction potential. Second, we obtain an effective 2D dynamics by integrating out the fast transverse motion of the molecules along the direction of the tight parabolic confinement.

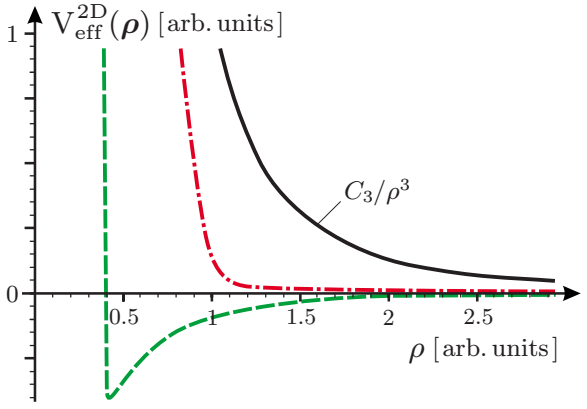


FIG. 2. (Color online) Qualitative sketch of effective 2D potentials $V_{\rm eff}^{\rm 2D}(\boldsymbol{\rho})$ for polar molecules confined in a 2D (pancake) geometry. Here, $\boldsymbol{\rho}=r\sin\vartheta(\cos\varphi,\sin\varphi)$ is the 2D coordinate in the plane $z=0$ and $\rho=r\sin\vartheta$ (see inset of Fig. 1). Solid line: Repulsive dipolar potential $V_{\rm eff}^{\rm 2D}(\boldsymbol{\rho})=C_3/\rho^3$ induced by a dc electric field. Dash-dotted line: Steplike potential induced by a single ac (microwave) field and a weak dc field. Dashed line: Attractive potential induced by the combination of several ac (microwave) fields and a weak dc field. Here, the potentials $V_{\rm eff}^{\rm 2D}(\boldsymbol{\rho})$ and the separation $\rho$ are given in arbitrary units. For the steplike case (dash-dotted line) $\rho=1$ corresponds to the Condon point $r_C$ of Sec. III C.

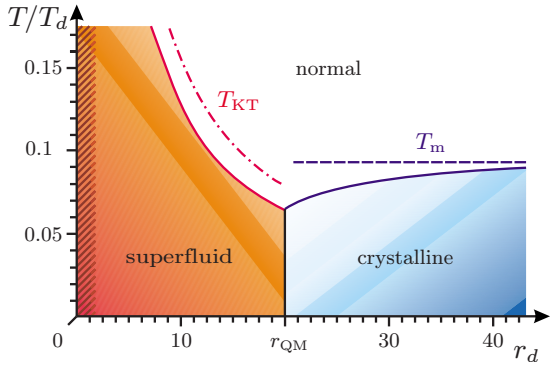


FIG. 3. (Color online) Sketch of the phase diagram for a homogeneous 2D system of polar molecules interacting via the effective 2D repulsive potential $V_{\rm eff}^{\rm 2D}(\boldsymbol{\rho})=C_3/\rho^3$. $T$ is the temperature in units of $T_d\equiv C_3/k_Ba^3$, with $a$ the average interparticle distance and $k_B$ the Boltzmann constant. The symbol $r_d\equiv E_{\rm int}/E_{\rm kin}=C_3m/\hbar^2a$ is the interaction ($E_{\rm int}=C_3/a^3$) to kinetic energy ($E_{\rm kin}=\hbar^2/ma^2$) ratio. A crystalline phase appears for large ratios $r_d>r_{\rm QM}$ and small temperatures $T<T_m$. The critical ratio $r_{\rm QM}\approx 18\pm4$ for the quantum melting to a superfluid phase has been determined in Ref. [31], while the classical melting temperature $T_m$ (dashed line) to a normal gas phase has been calculated in Ref. [37]. The finite-temperature superfluid to normal fluid phase transition is of the Berezinskii-Kosterlitz-Thouless type [38,39] and it appears below the upper bound $T_{\rm KT}=\pi\hbar^2/2k_Bma^2$ (dash-dotted line). The crossover to an unstable regime for small repulsion and finite confinement in the $z$ direction (see Fig. 1) is indicated by a hatched region (see text, Sec. III).

The paper is organized as follows. In Sec. II we discuss the Hamiltonian for a single rotating polar molecule dressed by dc and ac (microwave) fields under conditions of strong optical confinement. The collisions of two polar molecules are considered in Sec. III. After reviewing the molecular collisions in the absence of external fields, in Sec. III A we consider the case of interactions in the presence of a dc electric field. In particular, the stabilizing effects of a parabolic potential confining the particles to a 2D plane are analyzed in Secs. III A 3 and III A 4, while the effective 2D interaction potential $V_{\rm eff}^{\rm 2D}(\boldsymbol{\rho})=C_3/\rho^3$ is derived in Sec. III A 5. The interactions in the presence of an ac field are studied in Sec. III B. In the absence of external confinement, this case is analogous to the 3D optical shielding developed in the context of ultracold collisions of neutral atoms [40–42]. As in the latter, we find a strong dependence of the 3D shielding potential on the polarization of the ac field. The presence of "holes" in the 3D shielding potential for certain polarizations and of several degeneracies in the two-particle spectrum for all polarizations render the pure ac-field case less appealing for realizing stable collisional setups in 2D. In fact, both the former and the latter processes open loss channels for the ground-state interaction. In Sec. III C we analyze the interactions in combined dc and ac fields, and we show that the dc field helps to greatly suppress the presence of possible loss channels at large distances, while an additional harmonic confinement

along $z$ avoids populating the regions of space where "holes" analogous to those of Sec. III B occur. Thus, by introducing a *tight optical confinement* in the $z$ direction, in this case it is possible to realize *stable* two-dimensional collisional setups. Two-dimensional interparticle interactions can be designed, whose character varies markedly between long and short distances, allowing for much greater flexibility in tuning by external fields than the pure dc case of Sec. III A.

## II. MOLECULAR HAMILTONIANS

The purpose of this section, which forms the basis of discussion in the following sections, is to review the single-molecule rotational spectroscopy. In particular we are interested in the rotational excitations of cold $\nu^{2S+1}\Lambda(v)$ spinless $(S=0)$ polar molecules in their electronic $(\nu=0)$ and vibrational $(v=0)$ ground state, with zero projection $(\Lambda=0)$ of the total angular momentum on the internuclear axis [43,44]. The spectroscopic notation for the electronic-vibrational ground state of these molecules is $X\,^1\Sigma(0)$. Moreover, we are interested in manipulating the rotational states of these molecules using dc and ac electric fields and in confining the particles using a (optical) far-off-resonance trap (FORT). The application of these external fields will serve as a key element to engineer effective interaction potentials between the molecules.

Our goal in this section is to derive a low-energy effective Hamiltonian for the external motion and internal rotational excitations of a single molecule in its electronic-vibrational ground state of the form

$$H(t) = \frac{\mathbf{p}^2}{2m} + H_{\mathrm{rot}} + H_{\mathrm{dc}} + H_{\mathrm{ac}}(t) + H_{\mathrm{opt}}(\mathbf{r}).$$

In the last equation, $\mathbf{p}^2/2m$ is the kinetic energy for the center-of-mass motion of a molecule of mass $m$, while $H_{\mathrm{rot}}$ accounts for the rotational degrees of freedom. The terms $H_{\mathrm{dc}}$, $H_{\mathrm{ac}}(t)$, and $H_{\mathrm{opt}}(\mathbf{r})$ refer to the interaction with electric dc and ac (microwave) fields and to the optical trapping of the molecule in the ground electronic-vibrational manifold, respectively.

### A. Rotational excitations of $^1\Sigma$ molecules

We consider spinless polar molecules with $\Sigma$ electronic ground states in their electronic-vibrational ground state $X\,^1\Sigma(v=0)$. The low-energy internal excitations correspond to the rotation of the internuclear axis of the molecules with total internal angular momentum $\mathbf{J}$ [43–45]. The corresponding Hamiltonian $H_{\mathrm{rot}}$ is the one of a rigid spherical rotor [43]

$$H_{\mathrm{rot}} = B\mathbf{J}^2. \tag{1}$$

Here $B$ is the rotational constant for the electronic-vibrational ground state, which is of the order of $B \sim h \times 10$ GHz [46]. We denote the energy eigenstates of Eq. (1) by $|J,M\rangle$, where $J$ is the quantum number associated with the total internal angular momentum and $M$ is the quantum number associated with its projection onto a space-fixed quantization axis. The excitation spectrum is $E_J = BJ(J+1)$, which is anharmonic. Each $J$ level is $(2J+1)$-fold degenerate.

A polar molecule has an electric dipole moment $\mathbf{d}$ which couples its internal rotational levels. This dipole moment gives rise to the dipole-dipole interaction between two molecules. For $\Sigma$ molecules the dipole operator is along the internuclear axis $\mathbf{e}_{ab}$, i.e., $\mathbf{d} = d\mathbf{e}_{ab}$. Here, $d$ is the "permanent" dipole moment of a molecule in its electronic-vibrational ground state.

The spherical components of the dipole operator on a space-fixed spherical basis $\{\mathbf{e}_{-1}, \mathbf{e}_0, \mathbf{e}_1\}$, with $\mathbf{e}_{q=0} \equiv \mathbf{e}_z$ and $\mathbf{e}_{\pm 1} = \mp(\mathbf{e}_x \pm i\mathbf{e}_y)/\sqrt{2}$, are given by $d_q = \mathbf{e}_q \cdot \mathbf{d} = dC_q^{(1)}(\theta,\phi)$, where $C_q^{(k)}(\theta,\phi)$ are the unnormalized spherical harmonics and $\theta\,(\phi)$ is the polar (azimuthal) angle for the orientation of the molecule in the space-fixed frame [43–45], respectively. We note that for a spherically symmetric system, e.g., in the absence of external fields, the eigenstates of the rotor have no net dipole moment, $\langle J,M|\mathbf{d}|J,M\rangle = 0$. On the other hand, the component $d_q$ couples the rotational states $|J,M\rangle$ and $|J\pm 1, M+q\rangle$ according to

$$\langle J \pm 1, M+q|d_q|J,M\rangle = d(J,M;1,q|J\pm 1, M+q) \times (J,0;1,0|J\pm 1,0)\sqrt{\frac{2J+1}{2(J\pm 1)+1}},$$

where $(J_1,M_1;J_2,M_2|J,M)$ are the Clebsch-Gordan coefficients.

In the following we are interested in the interaction of the molecules with an external dc electric field along $\mathbf{e}_z$, $\mathbf{E}_{\mathrm{dc}} = E_{\mathrm{dc}}\mathbf{e}_0$, and with ac microwave fields with either linear polarization $(q=0)$ or circular polarization $(q=\pm 1)$ relative to $\mathbf{e}_z$, $\mathbf{E}_{\mathrm{ac}}(t) = E_{\mathrm{ac}}e^{-i\omega t}\mathbf{e}_q + \mathrm{c.c.}$ These fields couple to a molecule via the electric dipole interaction,

$$H_{\mathrm{dc}} = -\mathbf{d}\cdot\mathbf{E}_{\mathrm{dc}} = -d_0E_{\mathrm{dc}}, \tag{2a}$$

$$H_{\mathrm{ac}}(t) = -\mathbf{d}\cdot\mathbf{E}_{\mathrm{ac}}(t) = -d_qE_{\mathrm{ac}}e^{-i\omega t} + \mathrm{H.c.}, \tag{2b}$$

which try to align the molecule along the field, while competing with its rotation, as $[\mathbf{J}^2, d_q] \neq 0$.

### B. Coupling of rotational states by dc and ac electric fields

#### 1. Coupling to a dc electric field

The effects of a dc electric field $\mathbf{E}_{\mathrm{dc}}$ on a single polar molecule are (a) to split the $(2J+1)$-fold degeneracy in the rotor spectrum, and (b) to align the molecule along the direction of the field, which amounts to inducing a finite dipole moment in each rotational state.

We choose the direction of the dc field as the quantization axis, $\mathbf{E}_{\mathrm{dc}} \equiv E_{\mathrm{dc}}\mathbf{e}_0$. Then, the internal Hamiltonian is that of a rigid spherical pendulum [43,47],

$$H = H_{\mathrm{rot}} + H_{\mathrm{dc}} = B\mathbf{J}^2 - d_0E_{\mathrm{dc}}, \tag{3}$$

which conserves the projection of the angular momentum $J$ on the quantization axis, i.e., $M$ is a good quantum number. The energy eigenvalues and eigenstates of Eq. (3) are labeled as $E_{J,M}$ and $|\phi_{J,M}\rangle$, respectively.

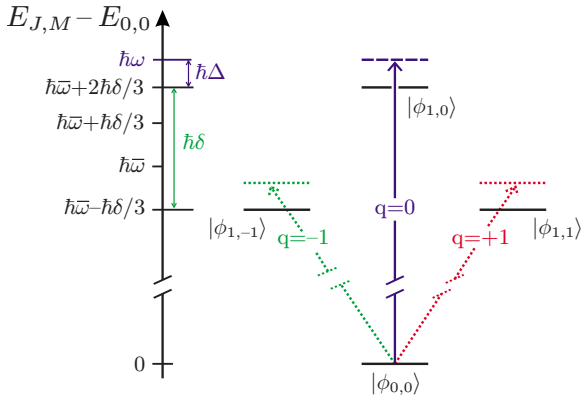


FIG. 4. (Color online) Solid lines: Energies $E_{J,M}$ (left) and states $|\phi_{J,M}\rangle$ (right) of Eq. (4) with $J=0,1$, for a molecule in a weak dc electric field $\mathbf{E}_{\rm dc}=E_{\rm dc}\mathbf{e}_0$ with $\beta\equiv dE_{\rm dc}/B\ll 1$. The dc-field-induced splitting $\hbar\delta$ and the average energy separation $\hbar\bar{\omega}$ are $\hbar\delta=3B\beta^2/20$ and $\hbar\bar{\omega}=2B+B\beta^2/6$, respectively. Dashed and dotted lines: Energy levels for a molecule in combined dc and ac fields (The ac Stark shifts of the dressed states are not shown). Dashed line: The ac field is monochromatic, with frequency $\omega$, linear polarization $q=0$, and detuning $\Delta=\omega-(\bar{\omega}+2\delta/3)>0$. Dotted lines: Schematics of energy levels for an ac field with polarization $q=\pm 1$ and frequency $\omega'\neq\omega$.

We are interested in weak fields, $E_{\rm dc}\ll B/d$, where the effects of the electric field are a quadratic dc Stark shift of the rotational energy levels and a finite induced dipole moment along the axis of the field in each rotational state. For a typical rotational constant $B\sim h\times 10$ GHz and a dipole moment $d\sim 9$ D, this corresponds to considering dc fields (much) weaker than $B/d\sim 2$ kV/cm. To lowest order in $\beta\equiv dE_{\rm dc}/B$ the energy eigenvalues and eigenstates are [43,47]

$$E_{J,M}/B=J(J+1)+\frac{\beta^2}{2}\frac{1-3M^2/J(J+1)}{(2J-1)(2J+3)}, \tag{4a}$$

$$|\phi_{J,M}\rangle=|J,M\rangle-\frac{\beta}{2J}\sqrt{\frac{J^2-M^2}{4J^2-1}}|J-1,M\rangle+\frac{\beta}{2(J+1)}\sqrt{\frac{(J+1)^2-M^2}{4(J+1)^2-1}}|J+1,M\rangle. \tag{4b}$$

Thus, the ground-state energy is shifted downward by $E_{0,0}=-B\beta^2/6$, while the energies of the lowest excited states are split by

$$\hbar\delta\equiv E_{1,0}-E_{1,\pm 1}=3B\beta^2/20 \tag{5}$$

(see the solid lines in Fig. 4). The average energy separation of the $J=0$ and $J=1$ manifolds is

$$\hbar\bar{\omega}=\sum_{M=-1}^{1}(E_{1,M}-E_{0,0})/3=2B+B\beta^2/6. \tag{6}$$

The induced dipole moments to lowest order in $\beta$ are

TABLE I. Permanent ($g_n$) and transition ($f_n$) dipole moments of the four states belonging to the rotational $J=0,1$ manifolds, in the presence of a weak polarizing dc field $\mathbf{E}_{\rm dc}=E_{\rm dc}\mathbf{e}_0$. Here, $\beta=dE_{\rm dc}/B\ll 1$ is the ratio of the electrostatic energy and rotational constant, and the dipole moments are given up to third order in $\beta$.

| | | |
|---|---|---|
| $g_0$ | $\langle\phi_{0,0}\|d_0\|\phi_{0,0}\rangle$ | $(d\beta/3)(1-11\beta^2/90)$ |
| $g_1$ | $\langle\phi_{1,\pm 1}\|d_0\|\phi_{1,\pm 1}\rangle$ | $(d\beta/10)/(1-19\beta^2/1400)$ |
| $g_2$ | $\langle\phi_{1,0}\|d_0\|\phi_{1,0}\rangle$ | $-(d\beta/5)(1-73\beta^2/350)$ |
| $f_0$ | $\langle\phi_{1,0}\|d_0\|\phi_{0,0}\rangle$ | $(d/\sqrt{3})(1-43\beta^2/360)$ |
| $f_1$ | $\langle\phi_{1,\pm 1}\|d_{\pm 1}\|\phi_{0,0}\rangle$ | $(d/\sqrt{3})(1-49\beta^2/1440)$ |
| $f_2$ | $\langle\phi_{1,0}\|d_{\mp 1}\|\phi_{1,\pm 1}\rangle$ | $(3d\beta/20)(1-577\beta^2/5600)$ |

$$\langle\phi_{J,M}|\mathbf{d}|\phi_{J,M}\rangle=d\beta\frac{3M^2/J(J+1)-1}{(2J-1)(2J+3)}\mathbf{e}_0.$$

This equation shows that the ground state acquires a finite dipole moment $g_0\equiv\langle\phi_{0,0}|d_0|\phi_{0,0}\rangle=d\beta/3$ along the field axis, while the lowest excited states acquire a dipole moment $\langle\phi_{1,M}|d_0|\phi_{1,M}\rangle=d(3M^2-2)\beta/10$. For later convenience, perturbative values in the small parameter $\beta$ of the transition and permanent dipole moments are reported in Table I for the four single-particle states $|\phi_{J,M}\rangle$ with $|M|\leq J\leq 1$. The transition and permanent dipole moments are labeled as $f_n$ and $g_n$, respectively.

#### 2. Coupling to an ac electric field

Similar to the case of a dc electric field, the basic effect of an ac electric field $\mathbf{E}_{\rm ac}$ on a single molecule is to polarize it by dressing its energy levels. The characteristic time dependence of the ac field allows for (a) addressing individual rotational transitions by applying one or several noninterfering microwave fields (multimode field); (b) realizing dressing fields that can be not only *linearly*, but also *circularly* polarized. In this work, we consider the case of a single ac microwave field with polarization $q$ and frequency $\omega$, $\mathbf{E}_{\rm ac}(\mathbf{r},t)=E_{\rm ac}(\mathbf{r})e^{-i\omega t}\mathbf{e}_q+$c.c., and derive the dressed energy levels for a molecule in the field. For the sake of generality—and for later convenience—we consider the case where the ac field is superimposed on a weak dc field, which provides for a splitting of the first excited $J=1$ manifold, as shown above.

Given a polarization $q$, the frequency $\omega$ is chosen close to the transition from the ground state to one state of the $J=1$ manifold, $|\phi_{0,0}\rangle\leftrightarrow|\phi_{1,q}\rangle$, i.e., $\omega\sim\bar{\omega}+\delta(2/3-q^2)$, where the states $|\phi_{J,M}\rangle$ are those of Eq. (4). The corresponding wavelength is of the order of centimeters, which greatly exceeds the size of our system and therefore one can neglect the position dependence of the microwave field, i.e., recoil effects, $E_{\rm ac}(\mathbf{r})\approx E_{\rm ac}$. The electric dipole interaction of Eq. (2b) reads

$$H_{\rm ac}(t)=-d_qE_{\rm ac}e^{-i\omega t}+\text{H.c.} \tag{7}$$

The Rabi frequency $\Omega$ and the detuning $\Delta$ are $\Omega\equiv E_{\rm ac}\langle\phi_{1,q}|d_q|\phi_{0,0}\rangle/\hbar=E_{\rm ac}f_{|q|}/\hbar$ and $\Delta\equiv\omega-(E_{1,q}-E_{0,0})/\hbar=\omega-[\bar{\omega}+\delta(2/3-q^2)]$, respectively (see Fig. 4).

In Sec. III we consider a specific setup where the ac field has linear polarization, $q=0$. Here we illustrate how to obtain the dressed energy levels of a molecule in this field by diagonalizing the Hamiltonian $H=H_{\rm rot}+H_{\rm dc}+H_{\rm ac}(t)$ in a Floquet picture. First, we expand the Hamiltonian on the basis $|\phi_{J,M}\rangle$, which diagonalizes the time-independent part of $H$ as $H_{\rm rot}+H_{\rm dc}=\Sigma_{J,M}|\phi_{J,M}\rangle E_{J,M}\langle\phi_{J,M}|$. Then, we consider the effect of the ac field driving the $|\phi_{0,0}\rangle\leftrightarrow|\phi_{1,0}\rangle$ transition with Rabi frequency $\Omega\equiv f_0E_{\rm ac}/\hbar\approx dE_{\rm ac}/\sqrt{3}\hbar$ and detuning $\Delta=\omega-(E_{1,0}-E_{0,0})/\hbar=\omega-2B(1+2\beta^2/15)/\hbar$.

A transformation to the Floquet picture is obtained by expanding the time-dependent wave function in a Fourier series in the ac frequency $\omega$. After applying a rotating wave approximation, i.e., keeping only the energy-conserving terms, we obtain the time-independent Hamiltonian $\tilde{H}$, which describes the coupled two-level system in the basis $\{|\phi_{0,0}\rangle,|\phi_{1,0}\rangle\}$ as

$$\tilde{H}=-\hbar\begin{bmatrix}0 & \Omega\\ \Omega & \Delta\end{bmatrix}+E_{0,0}.$$

The corresponding dressed energy eigenvalues of $\tilde{H}$ for the ground state and excited state (minus one photon energy $\hbar\omega$) are given by

$$\tilde{E}_{0,0}-E_{0,0}=-\frac{\hbar\Delta}{2}+\frac{\hbar\Delta}{2}\sqrt{1+\frac{4\Omega^2}{\Delta^2}}\approx+\frac{\hbar\Omega^2}{\Delta},$$

$$\tilde{E}_{1,0}-E_{0,0}=-\frac{\hbar\Delta}{2}-\frac{\hbar\Delta}{2}\sqrt{1+\frac{4\Omega^2}{\Delta^2}}\approx-\hbar\Delta-\frac{\hbar\Omega^2}{\Delta},$$

respectively. We note that the ac field induces an ac Stark shift $\approx\pm\hbar\Omega^2/\Delta$, on the ground and the excited states, respectively. Thus, the shift depends on the detuning $\Delta$, and in particular on its sign, and on the Rabi frequency $\Omega$.

### C. Optical trap

An essential ingredient of our setup is the tight confinement of the molecules in a 2D plane. This is realized, for example, by a far-off-resonant optical trap (see Fig. 1). The latter drives far-off-resonance transitions from $X\Sigma(0)$ to the electronically excited states $\nu\Lambda(v)$. The goal of this section is to obtain the resulting trapping potentials for the lowest rotational excitations, $J=0,1$.

A detailed discussion of the complex nature of molecular electronic excitations [43,44] is beyond the scope of the present discussion. For a detailed treatment of an example case, we refer to Ref. [48]. We consider here a simple model, where the fine and hyperfine interactions are neglected. Then the basic molecular structure is obtained as follows. In the adiabatic approximation one diagonalizes the Hamiltonian for the electrons and the two nuclei as a function of the internuclear separation $r_{ab}$, thus obtaining a set of Born-Oppenheimer potentials $E_{\nu\Lambda}(r_{ab})$. Here $\nu$ is the main electronic quantum number, while $\Lambda$ denotes the quantum number associated with the operator for the total angular momentum component of the molecules along the internuclear axis, $\mathbf{e}_{ab}\cdot\mathbf{J}$. The latter gives rise to a large splitting of the electronic manifolds $\sim A_\nu|\Lambda|^2$, where $A_\nu=\hbar^2/I_e$ is the inverse of the (small) moment of inertia of the electrons [43]. Then, the vibration of the nuclei in the BO potentials yields a series of bound states $v=0,1,2,\ldots$ with energy $E_{\nu\Lambda(v)}$.

Deep optical traps are obtained as follows. The laser, $\mathbf{E}_{\rm opt}(\mathbf{r},t)=\mathbf{E}_{\rm opt}(\mathbf{r})e^{-i\omega_{\rm L}t}+$c.c., drives the electronic transitions to the lowest excited states, labeled $A$ and $B$, with frequency $\omega_{\rm L}$ tuned near the minima of the BO potentials. Since spontaneous emission in the excited states is typically a few megahertz, deep traps on the order of 1 MHz with a negligible inelastic scattering rate ($\sim$ a few hertz) require detunings on the order of hundreds of gigahertz from the vibrational resonances. Since these detuning are much larger than $B$, one can neglect the rotational structure in the electronic ground and excited states in deriving the optical potential. The effective interaction of the molecules with the off-resonant laser field is thus described by

$$H_{\rm opt}(\mathbf{r})=-\mathbf{E}_{\rm opt}(\mathbf{r})^*\cdot\hat{\alpha}(\omega_{\rm L})\cdot\mathbf{E}_{\rm opt}(\mathbf{r}),\tag{8}$$

with the dynamic polarizability tensor

$$\begin{aligned}\hat{\alpha}(\omega_{\rm L})&=\alpha_\parallel(\omega_{\rm L})\mathbf{e}'_0\otimes\mathbf{e}'_0+\alpha_\perp(\omega_{\rm L})\sum_{\Lambda=\pm1}(-1)^\Lambda\mathbf{e}'_\Lambda\otimes\mathbf{e}'_{-\Lambda}\\&=\alpha_\perp(\omega_{\rm L})\sum_{q=-1}^{+1}(-1)^q\mathbf{e}_q\otimes\mathbf{e}_{-q}+[\alpha_\parallel(\omega_{\rm L})-\alpha_\perp(\omega_{\rm L})]\\&\quad\times\sum_{p,q}(-1)^{p-q}C^{(1)}_{-p}(\theta,\phi)C^{(1)}_q(\theta,\phi)\mathbf{e}_p\otimes\mathbf{e}_{-q}.\end{aligned}\tag{9}$$

Here $\{\mathbf{e}'_{-1},\mathbf{e}'_0,\mathbf{e}'_{+1}\}$ denotes a body-fixed spherical basis with $\mathbf{e}'_0\equiv\mathbf{e}_{ab}=\Sigma_q(-1)^qC^{(1)}_{-q}(\theta,\phi)\mathbf{e}_q$ being the internuclear axis, and $\alpha_\parallel(\omega_{\rm L})$ $[\alpha_\perp(\omega_{\rm L})]$ the dynamic polarizability at frequency $\omega_{\rm L}$ in the direction parallel (perpendicular) to the internuclear axis [43,49]. The parallel and perpendicular components are given by the $\Sigma$-$\Sigma$ ($\Delta\Lambda=0$) and $\Sigma$-$\Pi$ ($\Delta\Lambda=\pm1$) transitions, respectively, and read

$$\alpha_\parallel(\omega_{\rm L})=\sum_\pm\sum_{\nu,v}\frac{|d_{\nu\Sigma(v)\text{-}X\Sigma(0)}|^2}{E_{\nu\Sigma(v)}-E_{X\Sigma(0)}\mp\hbar\omega_{\rm L}},\tag{10a}$$

$$\alpha_\perp(\omega_{\rm L})=\sum_\pm\sum_{\nu,v}\frac{|d_{\nu\Pi(v)\text{-}X\Sigma(0)}|^2}{E_{\nu\Pi(v)}-E_{X\Sigma(0)}\mp\hbar\omega_{\rm L}}.\tag{10b}$$

Here $d_{\nu\Lambda(v)\text{-}X\Sigma(0)}$ denotes the transition dipole moment from $X\Sigma(0)$ to $\nu\Lambda(v)$, and the sum over $\mp$ accounts for the near-resonant and typically far off-resonant terms. From Eq. (10) we see that the anisotropy in the dynamic polarizabilities, $\alpha_\perp(\omega_{\rm L})-\alpha_\parallel(\omega_{\rm L})$, is due both to the different dipole moments and to the large splitting of the excited $\nu\Sigma(v)$ and $\nu\Pi(v)$ states.

In our setup we consider a pair of circularly polarized counter propagating laser beams, $\mathbf{E}_{\rm opt}(\mathbf{r})=E_{\rm opt}\cos(k_{\rm L}z)\mathbf{e}_+$, with wave vectors $\pm\mathbf{k}_{\rm L}=\pm\omega_{\rm L}\mathbf{e}_0/c$ along $z$, trapping the molecules in the $x$-$y$ plane (see Fig. 1). From Eq. (8) we obtain the following Hamiltonian for the optical trapping [49]:

$$H_{\rm opt}(\mathbf{r}) = -\alpha_0(\omega_{\rm L})|E_{\rm opt}|^2\cos^2(k_{\rm L}z)C_0^{(0)}(\theta,\phi) - \alpha_2(\omega_{\rm L})|E_{\rm opt}|^2\cos^2(k_{\rm L}z)C_0^{(2)}(\theta,\phi), \quad (11)$$

where $\alpha_0(\omega_{\rm L}) \equiv [\alpha_\parallel(\omega_{\rm L})+2\alpha_\perp(\omega_{\rm L})]/3$ and $\alpha_2(\omega_{\rm L}) \equiv [\alpha_\perp(\omega_{\rm L})-\alpha_\parallel(\omega_{\rm L})]/3$. The first term in Eq. (11), proportional to $C_0^{(0)}(\theta,\phi)=1$, gives an overall shift, which is common to all the rotational states. The second term is responsible for tensor shifts, which split the excited rotational states according to $|M|$, as

$$\langle J,M|C_0^{(2)}(\theta,\phi)|J,M\rangle = \frac{J(J+1)-3M^2}{(2J-1)(2J+3)}. \quad (12)$$

Typical depths of optical lattices are of the order of $\lesssim h \times 1$ MHz, and thus much smaller than $B$. Therefore we may neglect the far-off-resonant Raman coupling between different $J$ manifolds, i.e., $J \leftrightarrow J\pm 2$.

We consider *tight* optical traps, such that the molecules in the ground state are strongly confined at one potential minimum of $\langle\phi_{0,0}|H_{\rm opt}(\mathbf{r})|\phi_{0,0}\rangle = -\alpha_0(\omega_L)|E_{\rm opt}|^2\cos^2(k_Lz)$. For a light field which is (far) red detuned from the electronic excited states, i.e., $\hbar\omega_{\rm L} \ll E_{\nu\Lambda(v)}-E_{X\Sigma(0)}$, the dynamic polarizabilities $\alpha_\parallel(\omega_{\rm L})$ and $\alpha_\perp(\omega_{\rm L})$ are positive and the trapping potential for the ground state is attractive, since $\alpha_0(\omega_{\rm L})>0$. We assume the molecule to be strongly confined near the field antinode $z=0$. Then the optical trapping is essentially given by a tight harmonic trap,

$$H_{\rm opt}(\mathbf{r}) \approx -\alpha_0(\omega_{\rm L})|E_{\rm opt}|^2(1-k^2z^2) - \alpha_2(\omega_{\rm L})|E_{\rm opt}|^2(1-k_{\rm L}^2z^2)C_0^{(2)}(\theta,\phi). \quad (13)$$

From the last expression we see that the tensor shifts induce a position-dependent splitting for the excited rotational manifolds, which at $z=0$ is analogous to that induced by a dc field, but has a strong modulation in space. The tensor shifts are thus seen as position- and state-dependent potentials, and the last term in $H_{\rm opt}(\mathbf{r})$ is (in principle) unwanted for our purposes, since it gives rise to different trapping frequencies $\omega_\perp$ for the ground and excited states.

However, we note that by applying a second laser, $\mathbf{E}'_{\rm opt}(\mathbf{r},t)$, of frequency $\omega'_{\rm L}$ with wave vector $\mathbf{k}'_{\rm L}$ and polarization $\mathbf{e}'_{\rm L}$, one can eliminate the state-dependent potentials—up to a position-independent splitting of the excited states. Given the large number and variety of available excited electronic-vibrational states, several choices are possible. One choice is, e.g., to apply an additional laser with the same polarization $\mathbf{e}'_{\rm L}$ as the first laser, i.e., $\mathbf{e}'_{\rm L}=\mathbf{e}_+$, but having a node at $z=0$ and being blue detuned from the electronic transitions, i.e., $E'_{\rm opt}(\mathbf{r},t)=E'_{\rm opt}\sin(k'_{\rm L}z)e^{-i\omega'_{\rm L}t}\mathbf{e}_+ + \text{c.c.}$ with $\omega'_{\rm L} \gg (E_{\nu\Lambda(0)}-E_{X\Sigma(0)})/\hbar$ for $\nu\Lambda = A\Pi, B\Sigma$. This induces an additional state-dependent optical trapping potential given by $H'_{\rm opt}(\mathbf{r}) = -|E'_{\rm opt}|\sin^2(k'_{\rm L}z)[\alpha_0(\omega'_{\rm L})+\alpha_2(\omega'_{\rm L})C_0^{(2)}(\theta,\phi)]$. Tuning the laser frequency $\omega'_{\rm L}$ with respect to the vibrational resonances one can force both $\alpha_\perp(\omega'_{\rm L})$ and $\alpha_\parallel(\omega'_{\rm L})$ to be negative [see Eq. (10)]. The additional trapping potentials are zero at their node $z=0$; in particular, for the ground state the trapping potential is repulsive (thus enhancing the trapping given by the first laser), while the excited-state position-dependent trapping $\propto z^2C_0^{(2)}(\theta,\phi)$ of Eq. (13) can be compensated for by tuning the strength of the second laser, $E'_{\rm opt}$.

The parabolic trapping potential for our setup is then given by

$$H_{\rm opt}(\mathbf{r}) = \frac{1}{2}m\omega_\perp^2z^2 - V_0 - V_2C_0^{(2)}(\theta,\phi), \quad (14)$$

where the first term is a state-independent harmonic trapping along $\mathbf{e}_z$ at frequency

$$\omega_\perp = \sqrt{2[\alpha_0(\omega_{\rm L})|E_{\rm opt}k_{\rm L}|^2 + |\alpha_0(\omega'_{\rm L})||E'_{\rm opt}k'_{\rm L}|^2]/m},$$

the second terms gives an overall Stark shift $V_0 = \alpha_0(\omega_{\rm L})|E_{\rm opt}|^2$, and the last term is a splitting of the excited rotational states, $J>0$, which is independent of the position $z$, $V_2=\alpha_2(\omega_{\rm L})|E_{\rm opt}|^2$.

Concluding, the Hamiltonian for a single molecule is

$$H(t) = \frac{\mathbf{p}^2}{2m} + \frac{1}{2}m\omega_\perp^2z^2 - V_0 - V_2C_0^{(2)}(\theta,\phi) + B\mathbf{J}^2 - d_0E_{\rm dc} - (d_qE_{\rm ac}e^{-i\omega t} + \text{H.c.}). \quad (15)$$

## III. TWO MOLECULES

We consider the interactions of two polar molecules $j=1,2$ confined to the $x$-$y$ plane by a tight harmonic trapping potential of frequency $\omega_\perp$, directed along $z$. The interaction of the two molecules at a distance $\mathbf{r}\equiv\mathbf{r}_2-\mathbf{r}_1=r\mathbf{e}_r$ is described by the Hamiltonian

$$H(t) = \sum_{j=1}^{2} H_j(t) + V_{\rm dd}(\mathbf{r}), \quad (16)$$

where $H_j(t)$ is the single-molecule Hamiltonian Eq. (15), and $V_{\rm dd}(\mathbf{r})$ is the dipole-dipole interaction

$$V_{\rm dd}(\mathbf{r}) = \frac{\mathbf{d}_1\cdot\mathbf{d}_2 - 3(\mathbf{d}_1\cdot\mathbf{e}_r)(\mathbf{e}_r\cdot\mathbf{d}_2)}{r^3}. \quad (17)$$

Here, $\mathbf{d}_j$ is the dipole operator of the molecule $j$, and $\mathbf{e}_r\cdot\mathbf{d}_j$ is its projection onto the collision axis $\mathbf{e}_r$. The projection reads $\mathbf{e}_r\cdot\mathbf{d}_j = \Sigma_{q=-1}^{+1}(-1)^qC_{-q}^{(1)}(\vartheta,\varphi)d_{q;j}$, where $C_q^{(1)}(\vartheta,\varphi)\equiv\mathbf{e}_q\cdot\mathbf{e}_r$ are unnormalized spherical harmonics with $\vartheta$ and $\varphi$ polar and azimuthal angles relating the orientation of $\mathbf{e}_r$ with respect to a space-fixed frame $\mathbf{e}_q$, respectively. The terms $d_{q;j}\equiv\mathbf{e}_q\cdot\mathbf{d}_j$ are the spherical components of the projection of the dipole operator of molecule $j$ onto the space-fixed frame $\mathbf{e}_q$.

In the absence of external fields $E_{\rm dc}=E_{\rm ac}=0$, the interaction of the two molecules in their rotational ground state is determined by the van der Waals attraction $V_{\rm vdW}\sim C_{6;0}/r^6$ with $C_{6;0}\approx -d^4/6B$. This expression for the interaction potential is valid outside of the molecular core region $r>r_B \equiv (d^2/B)^{1/3}$, where $r_B$ defines the characteristic length where the dipole-dipole interaction becomes comparable to the splittings of the rotational levels (see below). In the following we show that it is possible to *induce* and *design* interaction potentials that are long range, by dressing the interac-

tions with appropriately chosen static and/or microwave fields. In fact, the combination of the latter with low-dimensional trapping allows one to engineer effective potentials whose *strength* and *shape* can both be tuned. The derivation of the effective interactions proceeds in two steps. (i) We derive a set of Born-Oppenheimer potentials by first separating Eq. (16) into center-of-mass and relative coordinates, and diagonalizing the Hamiltonian for the relative motion for fixed molecular positions. Within an adiabatic approximation, the corresponding eigenvalues play the role of an effective 3D interaction potential in a given state manifold dressed by the external field. (ii) We eliminate the motional degrees of freedom in the tightly confined $z$ direction to obtain an effective 2D dynamics with interaction $V_{\mathrm{eff}}^{\mathrm{2D}}(\boldsymbol{\rho})$. In the following we consider the cases of a static field and a microwave field, coupling the lowest rotor states.

### A. Effective interactions in the presence of a dc electric field

In this section we consider the collisions of two ground-state molecules in the presence of a dc electric field $\mathbf{E}_{\mathrm{dc}}=E_{\mathrm{dc}}\mathbf{e}_0$. The Hamiltonian Eq. (16) now reads

$$H=\sum_{j=1}^{2}\left(\frac{\mathbf{p}_j^2}{2m}+\frac{1}{2}m\omega_\perp^2 z_j^2+B\mathbf{J}_j^2-E_{\mathrm{dc}}d_{0;j}\right)+V_{\mathrm{dd}}(\mathbf{r})$$
$$=\sum_{j=1}^{2}\left(\frac{\mathbf{p}_j^2}{2m}+\frac{1}{2}m\omega_\perp^2 z_j^2\right)+H_{\mathrm{int}}(\mathbf{r}), \tag{18}$$

where $d_{0;j}=\mathbf{e}_0\cdot\mathbf{d}_j$ and $H_{\mathrm{int}}(\mathbf{r})$ is the internal Hamiltonian including the dipole-dipole interaction, $H_{\mathrm{int}}(\mathbf{r})=\Sigma_j(B\mathbf{J}_j^2-E_{\mathrm{dc}}d_{0;j})+V_{\mathrm{dd}}(\mathbf{r})$, respectively. In this section we are interested in ground-state collisions, and thus for convenience we set $V_2=0$ in Eq. (18), that is, we neglect possible tensor shifts in the excited-state energies of each molecule. We can further rewrite Eq. (18) by splitting $H$ into center-of-mass and relative coordinates as $H=H_{\mathrm{com}}+H_{\mathrm{rel}}$ with

$$H_{\mathrm{com}}=\frac{\mathbf{P}^2}{4m}+m\omega_\perp^2 Z^2, \tag{19a}$$

$$H_{\mathrm{rel}}=\frac{\mathbf{p}^2}{m}+\frac{1}{4}m\omega_\perp^2 z^2+H_{\mathrm{int}}(\mathbf{r}). \tag{19b}$$

Here, $\mathbf{R}=(\mathbf{r}_1+\mathbf{r}_2)/2$ and $\mathbf{P}=\mathbf{p}_1+\mathbf{p}_2$ are the center-of-mass coordinate and momentum of the two molecules, while $\mathbf{r}=\mathbf{r}_2-\mathbf{r}_1$ and $\mathbf{p}=(\mathbf{p}_2-\mathbf{p}_1)/2$ are the relative coordinate and momentum, respectively. Equations (19) show that the dipole-dipole interaction couples the internal degrees of freedom to the relative motion, while the latter and the harmonic motion of the center of mass remain decoupled. Thus, the nontrivial system's dynamics is entirely determined by $H_{\mathrm{rel}}$. In the following we focus our discussion on this term.

As explained above, in the spirit of the BO approximation we can obtain effective interaction potentials for the collision of the two particles by diagonalizing $H_{\mathrm{rel}}$ for fixed particle positions and zero kinetic energy. In the adiabatic approximation, the resulting eigenvalues are energy surfaces which act as effective potentials in each state manifold. Here we first analyze the case of collisions in the absence of external fields, that is, $E_{\mathrm{dc}}=\omega_\perp=0$ (Sec. III A 1). Then, in Sec. III A 2 we add a static electric field of small strength $E_{\mathrm{dc}}\ll B/d$. The effects of finite trapping $\omega_\perp\neq 0$ are treated in the following section, Sec. III A 3 for the most relevant case of ground-state collisions. The stability of ground-state collisions is investigated in Sec. III A 4. The effective two-dimensional potential for ground-state collision is derived in Sec. III A 5.

#### 1. Collisions in the absence of external fields

In the absence of external fields ($E_{\mathrm{dc}}=\omega_\perp=0$) and for zero kinetic energy, diagonalizing $H_{\mathrm{rel}}$ amounts to diagonalizing $H_{\mathrm{int}}(\mathbf{r})$ as a function of $\mathbf{r}$,

$$H_{\mathrm{int}}(\mathbf{r})=\sum_{j=1}^{2}B\mathbf{J}_j^2+V_{\mathrm{dd}}(\mathbf{r})=\sum_n|\Phi_n(\mathbf{r})\rangle E_n(\mathbf{r})\langle\Phi_n(\mathbf{r})|, \tag{20}$$

where $E_n(\mathbf{r})$ and $|\Phi_n(\mathbf{r})\rangle$ are the $n$th adiabatic energy eigenvalues and two-particle eigenfunctions, respectively, and $n$ is a collective index for a set of quantum numbers to be specified below. Each eigenvalue $E_n(\mathbf{r})$ plays the role of an effective interaction in a given state manifold dressed by the external field. At infinite separations of the molecules, the eigenfunctions $|\Phi_n^{(0)}(\mathbf{r})\rangle\equiv|\Phi_n^{(0)}(\vartheta,\varphi)\rangle=|\Phi_n(r\to\infty,\vartheta,\varphi)\rangle$ are symmetrized products of the (rotated) single-particle eigenstates $|J_j,M_j\rangle_j'\equiv e^{-i\varphi J_{z;j}}e^{-i\vartheta J_{y;j}}|J_j,M_j\rangle_j$, which are independent of the distance $r$. For finite $r$ the two-particle eigenstates are superposition of several single-particle states, which are mixed by the dipole-dipole interaction $V_{\mathrm{dd}}(\mathbf{r})$.

A few eigenvalues $E_n(\mathbf{r})$ of Eq. (20) are plotted as a function of $\mathbf{r}$ in Fig. 5. Figure 5 shows that the energy spectrum behaves quite differently for $r<r_B$ and $r>r_B$, $r_B\equiv(d^2/B)^{1/3}$. In fact, for $r<r_B$ a large number of level crossings and anticrossings occurs, which make the satisfaction of the adiabatic approximation generally impossible. The region $r<r_B$ is the *molecular core* region. In the following we focus on the region $r>r_B$, where the lowest-energy eigenvalues group into well-defined manifolds, which are approximately spaced by an energy $\approx 2B$. For ground-state collisions, the adiabatic approximation is here trivially satisfied.

Since we are interested in ground-state collisions, we restrict our discussion to the $J_j=0$ and 1 manifolds of each molecule, which amounts to taking into account 16 rotational two-particle states. The corresponding eigenvalues $E_n(\mathbf{r})$ are clearly distinguishable in Fig. 5 in the region $r>r_B$. The manifolds are approximately split by $2B$, according to the number of rotational excitations $J_1+J_2$ shared by the two molecules. The two-particle energy eigenstates and eigenpotentials can be classified according to the following symmetries of $H_{\mathrm{int}}(\mathbf{r})$. (a) The projection of the total internal angular momentum along the collision axis, $\mathbf{e}_r\cdot(\mathbf{J}_1+\mathbf{J}_2)$, is conserved and associated with a quantum number $Y$. (b) The Hamiltonian is invariant under the exchange of the two particles, which is associated with the permutation symmetry $\sigma=\pm$ under the exchange of the two particles. This implying that symmetric (antisymmetric) states couple to symmetric (antisymmetric) states only. (c) The parity $p=\sigma(-1)^{J_1+J_2}$ is con-

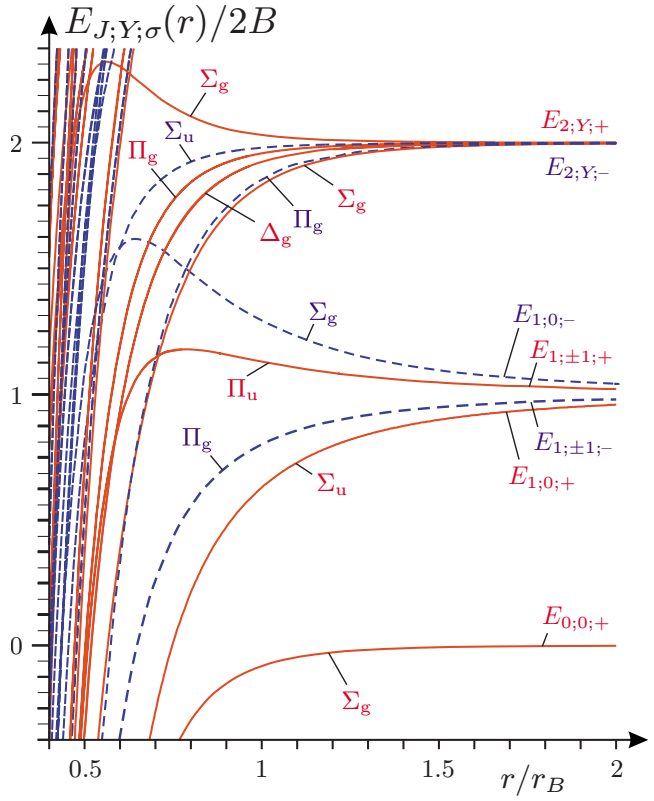


FIG. 5. (Color online) BO potentials $E_{J;Y;\sigma}(\mathbf{r})$ as a function of the distance $r$, for two molecules interacting in the absence of external fields, $E_{dc}=\omega_\perp=\beta=0$ (see text and Table II). Here, $J=J_1+J_2$, $Y$, and $\sigma$ are the total number of rotational excitations shared by the two molecules, the quantum number associated with the projection of the total internal angular momentum onto the collision axis $\mathbf{e}_r\cdot(\mathbf{J}_1+\mathbf{J}_2)$, and the permutation symmetry under the exchange of the particles, respectively. The solid and dashed curves correspond to symmetric ($\sigma=+$) and antisymmetric ($\sigma=-$) eigenstates, respectively. Each potential energy surface is labeled by the corresponding energy and eigenstate (see Table II). Here, $r_B\equiv(d^2/B)^{1/3}$, with $d$ the permanent dipole moment and $B$ the rotational constant of each molecule, respectively. Note that the $\Pi$ and $\Delta$ states are doubly degenerate.

served. The spectroscopic notations labeling the eigenstates $|\Phi_n(\mathbf{r})\rangle$ and potentials $E_n(\mathbf{r})$,with $n\equiv(J=J_1+J_2;Y;\sigma)$ in Fig. 5 are explained in the caption of Table II.

Analytic results for the energy eigenvalues and eigenstates of $H_{int}(\mathbf{r})$ for large enough interparticle distances $r$ can be derived using a perturbative expansion in $V_{dd}(\mathbf{r})/B$. Our results for the energy eigenvalues $E_n(\mathbf{r})\equiv E_{J_1+J_2;Y;\sigma}(\mathbf{r})$ of $B\Sigma_j\mathbf{J}_j^2+V_{dd}(\mathbf{r})$ are summarized in Table II. There, the asymptotic energies $E_n^{(0)}\equiv E_n(r\to\infty)$, the dipole-dipole coefficients $C_{3;n}$, and the van der Waals coefficients $C_{6;n}$ are reported, so that the perturbative expressions for $E_n(\mathbf{r})$ take the form $E_n(\mathbf{r})=E_n^{(0)}+C_{3;n}/r^3+C_{6;n}/r^6$. The table shows that the ground-state energy $E_0(\mathbf{r})\equiv E_{0;0;+}(\mathbf{r})$ is shifted downward by an amount $E_{0;0;+}(\mathbf{r})=-d^4/6Br^6$, which is the usual van der Waals shift due to off-resonant dipole-dipole interactions. The first excited manifold ($J_1+J_2=1$) consists of six states, of which three are symmetric and three are antisymmetric. These states are split by the resonant dipole-dipole interaction according to their angular momentum along the collision axis, $|Y|=0,1$ and $\sigma=\pm$, as reported in Table II. Finally, the second excited manifold ($J_1+J_2=2$) consists of nine states, of which six are symmetric, $Y=0_\pm,\pm1,\pm2$ with $\sigma=+$, and three are antisymmetric, $Y=0,\pm1$ with $\sigma=-$.

#### 2. Collisions in a dc field: Effective 3D interaction

We now turn to study the collision of the two molecules in the presence of a weak static electric field applied in the $z$ direction but in the absence of optical trapping, that is, $\mathbf{E}=E_{dc}\mathbf{e}_0$ with $E_{dc}\ll B/d$ and $\omega_\perp=0$. As explained in Sec. II B 1, the effects of a dc electric field on each molecule are to partially split the $(2J+1)$-fold degeneracy in the rotor spectrum (the modulus of the projection $M$ is conserved), and to align the molecule along the direction of the field, which amounts to inducing a finite dipole moment ${}_j\langle\phi_{J_j,M_j}|d_{0;j}|\phi_{J_j,M_j}\rangle_j$ in each rotational state.

Analogous to the discussion above, the effective interaction potentials for the collision of the two particles can be obtained in the adiabatic approximation by diagonalizing the Hamiltonian $H_{rel}=H_{int}(\mathbf{r})=\Sigma_{j=1}^2(B\mathbf{J}_j^2-E_{dc}d_{0;j})+V_{dd}(\mathbf{r})=\Sigma_n|\Phi_n(\mathbf{r})\rangle E_n(\mathbf{r})\langle\Phi_n(\mathbf{r})|$, where now the asymptotic energy eigenstates $|\Phi_n^{(0)}(\vartheta,\varphi)\rangle$ are symmetrized products of the single-particle states $|\phi_{J_j,M_j}\rangle_j$ of Eq. (4). The quantity $n\equiv(J;M;\sigma)$ is the collective quantum number labeling the eigenvalues $E_n(\mathbf{r})$, with $J=J_1+J_2$, $M\equiv|M_1|+|M_2|$, and $\sigma=\pm$. We note that, because of the presence of the dc field, here $J$ is a simple label for the various energy manifolds, and not a quantum number. The energies of the eigenvalues $E_n(\mathbf{r})$ and the associated eigenvectors are tabulated in Table III.

Similar to the zero-field discussion, in the weak-field limit $\beta\ll1$, and for $r>r_B$ we expect the eigenvalues of $H_{int}(\mathbf{r})$ to group into manifolds, which are approximately separated by the rotational spacing $2B$. On the other hand, because of the finite induced dipole moments ${}_j\langle\phi_{J_j,M_j}|d_{0;j}|\phi_{J_j,M_j}\rangle_j$, the two molecules can now interact resonantly via the dipole-dipole interaction $V_{dd}(\mathbf{r})$ in each state manifold. This has important consequences for ground-state collisions. In fact, the new effective ground-state potential $E_0(\mathbf{r})$ derived in perturbation theory in $V_{dd}(\mathbf{r})/B$ reads

$$V_{eff}^{3D}(\mathbf{r})\equiv E_0(\mathbf{r})\approx\frac{C_{3;0}}{r^3}(1-3\cos^2\vartheta)+\frac{C_{6;0}}{r^6},\qquad(21)$$

where a constant term $2E_{0,0}=-\beta^2B/3$ due to single-particle dc Stark shifts has been neglected. The constants $C_{3;0}\approx d^2\beta^2/9$ and $C_{6;0}\approx-d^4/6B$ are the dipolar and van der Waals coefficients for the ground state, respectively (see Table III). Equation (21) is valid for $r\gg r_B$, and it shows that for distances $r\gg r_\star$ with

$$r_\star\equiv\left(\frac{2|C_{6;0}|}{C_{3;0}}\right)^{1/3}\approx\left(\frac{3d^2}{B\beta^2}\right)^{1/3}\qquad(22)$$

the dipole-dipole interaction dominates over the van der Waals attractive potential, and $V_{eff}^{3D}(\mathbf{r})\sim C_{3;0}(1-3\cos^2\vartheta)/r^3$ [31]. In fact, the potential has a local maximum in the plane $z=r\cos\vartheta=0$ at the position $r=r_\star$, where the dipole-dipole

TABLE II. Perturbative expansions of the effective potentials, $E_n \equiv E_{J;Y;\sigma}$, for the three lowest-energy manifolds, $J=J_1+J_2=0,1,2$ with $J_j=0,1$, for interactions in the absence of external fields $E_{\rm dc}=E_{\rm ac}=\omega_\perp=0$. First column: index $n=0,1,2,\ldots$ labeling the energy potentials and states. Second column: total number of rotational excitations shared by the two molecules, $J=J_1+J_2$. Third column: the quantum number $Y$ associated with the projection of the total internal angular momentum along the collision axis $\mathbf{e}_r\cdot(\mathbf{J}_1+\mathbf{J}_2)$, which is denoted by $\Sigma,\Pi,\Delta$ for $Y=0,1,2$, respectively. For $n=7,8$ the subindex $\pm$ indicates the presence of two states, which are split by the van der Waals interaction. Fourth column: permutation symmetry $\sigma=\pm$. Fifth column: spectroscopic notation with parity $p=\sigma(-1)^J$ denoted by $g$ (gerade) for $p=+1$ and $u$ (ungerade) for $p=-1$, respectively. Sixth column: Asymptotic energy $E_n^{(0)} \equiv E_n(r\to\infty)$. Seventh column: dipole-dipole coefficient $C_{3;n}$. Last column: van der Waals coefficient $C_{6;n}$. Perturbative energy eigenvalues are expressed in the form $E_n(\mathbf{r})=E_n^{(0)}+C_{3;n}/r^3+C_{6;n}/r^6$.

| $n$ | $J$ | $Y$ | $\sigma$ | $Y_p$ | $E_n^{(0)}$ | $C_{3;n}/d^2$ | $C_{6;n}\times 6B/d^4$ |
|---|---|---|---|---|---|---|---|
| 0 | 0 | 0 | + | $\Sigma_g$ | 0 | 0 | −1 |
| 1 | 1 | 0 | + | $\Sigma_u$ | $2B$ | −2/3 | −22/45 |
| 2,3 | 1 | ±1 | − | $\Pi_g$ | $2B$ | −1/3 | −19/45 |
| 4,5 | 1 | ±1 | + | $\Pi_u$ | $2B$ | +1/3 | −19/45 |
| 6 | 1 | 0 | − | $\Sigma_g$ | $2B$ | +2/3 | −22/45 |
| 7,8 | 2 | $0_\pm$ | + | $\Sigma_g$ | $4B$ | 0 | $-(48\mp 39\sqrt{3})/50$ |
| 9,10 | 2 | ±1 | − | $\Pi_u$ | $4B$ | 0 | −39/20 |
| 11,12 | 2 | ±2 | + | $\Delta_g$ | $4B$ | 0 | −24/25 |
| 13,14 | 2 | ±1 | + | $\Pi_g$ | $4B$ | 0 | −51/25 |
| 15 | 2 | 0 | − | $\Sigma_u$ | $4B$ | 0 | −6/25 |

TABLE III. Perturbative expressions for the 16 lowest-energy BO potentials $E_n(\mathbf{r})=E_n^{(0)}+C_{3;n}h_n(\vartheta)/r^3+C_{6;n}(\vartheta)/r^6$ of two molecules interacting in the presence of a dc electric field $\mathbf{E}_{\rm dc}=(B\beta/d)\mathbf{e}_0$. First column: collective quantum number $n\equiv(J=J_1+J_2;M\equiv|M_1|+|M_2|;\sigma=\pm)$ labeling the eigenstates $E_n(\mathbf{r})$. Second column: number $J=J_1+J_2$ of rotational excitations shared by the two molecules. Because of the presence of the dc field, parity is not conserved and $J$ is a simple index that labels the various energy manifolds for $r\gg r_B, r_\delta$. Third column: quantum number $M\equiv|M_1|+|M_2|$. The additional subindex $\mu$ for $M>0$ labels superposition of states with the same $(Y;M;\sigma)$, which depend on the azimuthal angle $\varphi$ (see eighth column). Fourth column: quantum number $\sigma=+$ $(\sigma=-)$ denoting symmetric (antisymmetric) states under permutation of the two molecules. Fifth column: asymptotic energies $E_n^{(0)}$ for infinite separation. The quantities $\hbar\delta$ and $\hbar\bar{\omega}$ are defined in Eqs. (5) and (6), respectively. Sixth column: $C_{3;n}$ coefficient and the angular dependence $h_n(\vartheta)$. The dipole moments $g_n$ and $f_n$ are defined in Table I, while the angular distribution $\Upsilon$ is $\Upsilon\equiv 1-3\cos^2\vartheta$. Seventh column: contributions to the $C_{6;n}(\vartheta)$ coefficient up to order $O(\beta^2)$. The values $A_1$, $A_2$, and $A_3$ are $A_1\equiv 40(2-\Upsilon-\Upsilon^2)(f_0f_1+f_2g_0)^2/d^4\beta^2$, $A_2\equiv 33+6\Upsilon-\Upsilon^2/2$, $A_3\equiv 13(1+\Upsilon)/\cos\xi$, respectively. Here, $\xi$ is defined by the relation $\tan\xi=(14-\Upsilon)(2+\Upsilon)/26(1+\Upsilon)$. Last column: eigenstates $|\Phi_n^{(0)}(\vartheta,\varphi)\rangle\equiv|\Phi_n(r\to\infty,\vartheta,\varphi)\rangle$ valid at infinite separation. Here, "perm." denotes the permuted state, e.g., $|\phi_{1,2};\phi_{3,4}\rangle\to|\phi_{3,4};\phi_{1,2}\rangle$.

| $n$ | $J$ | $M_\mu$ | $\sigma$ | $E_n^{(0)}-2E_{0,0}$ | $C_{3;n}h_n(\vartheta)$ | $C_{6;n}(\vartheta)6B/d^4$ | $\lvert\Phi_n^{(0)}(\vartheta,\varphi)\rangle$ |
|---|---|---|---|---|---|---|---|
| 0 | 0 | 0 | + | 0 | $g_0^2\Upsilon$ | −1 | $\lvert\phi_{0,0};\phi_{0,0}\rangle$ |
| 1 | 1 | $1_-$ | + | $\hbar(\bar{\omega}-\delta/3)$ | $(g_0g_1-f_1^2)\Upsilon-f_1^2$ | $-A_1-(21+\Upsilon)/45$ | $\Sigma_\pm\pm e^{\mp i\varphi}\lvert\phi_{0,0};\phi_{1,\pm1}\rangle/2+$perm. |
| 2 | 1 | $1_-$ | − | $\hbar(\bar{\omega}-\delta/3)$ | $(g_0g_1+f_1^2)\Upsilon+f_1^2$ | $-A_1-(21+\Upsilon)/45$ | $\Sigma_\pm\pm e^{\mp i\varphi}\lvert\phi_{0,0};\phi_{1,\pm1}\rangle/2-$perm. |
| 3 | 1 | $1_+$ | + | $\hbar(\bar{\omega}-\delta/3)$ | $g_0g_1\Upsilon+f_1^2$ | −19/45 | $\Sigma_\pm e^{\mp i\varphi}\lvert\phi_{0,0};\phi_{1,\pm1}\rangle/2+$perm. |
| 4 | 1 | $1_+$ | − | $\hbar(\bar{\omega}-\delta/3)$ | $g_0g_1\Upsilon-f_1^2$ | −19/45 | $\Sigma_\pm e^{\mp i\varphi}\lvert\phi_{0,0};\phi_{1,\pm1}\rangle/2-$perm. |
| 5 | 1 | 0 | + | $\hbar(\bar{\omega}+2\delta/3)$ | $(g_0g_2+f_0^2)\Upsilon$ | $+A_1-(20-\Upsilon)/45$ | $\lvert\phi_{0,0};\phi_{1,0}\rangle/\sqrt{2}+$perm. |
| 6 | 1 | 0 | − | $\hbar(\bar{\omega}+2\delta/3)$ | $(g_0g_2-f_0^2)\Upsilon$ | $+A_1-(20-\Upsilon)/45$ | $\lvert\phi_{0,0};\phi_{1,0}\rangle/\sqrt{2}-$perm. |
| 7 | 2 | 2 | − | $2\hbar(\bar{\omega}-\delta/3)$ | $g_1^2\Upsilon$ | $-3(46+19\Upsilon)/100$ | $\Sigma_\pm\pm\lvert\phi_{1,\pm1};\phi_{1,\mp1}\rangle/\sqrt{2}$ |
| 8 | 2 | $2_-$ | + | $2\hbar(\bar{\omega}-\delta/3)$ | $g_1^2\Upsilon$ | $-3(22-5\Upsilon)/100$ | $\Sigma_\pm\pm e^{\mp 2i\varphi}\lvert\phi_{1,\pm1};\phi_{1,\pm1}\rangle/\sqrt{2}$ |
| 9 | 2 | $2_0$ | + | $2\hbar(\bar{\omega}-\delta/3)$ | $g_1^2\Upsilon$ | $-3(A_2+A_3)/100$ | $\Sigma_\pm(c_\xi\lvert\phi_{1,\pm1};\phi_{1,\mp1}\rangle-s_\xi e^{\mp 2i\varphi}\lvert\phi_{1,\pm1};\phi_{1,\pm1}\rangle)/\sqrt{2}$ |
| 10 | 2 | $2_+$ | + | $2\hbar(\bar{\omega}-\delta/3)$ | $g_1^2\Upsilon$ | $-3(A_2-A_3)/200$ | $\Sigma_\pm(s_\xi\lvert\phi_{1,\pm1};\phi_{1,\mp1}\rangle+c_\xi e^{\mp 2i\varphi}\lvert\phi_{1,\pm1};\phi_{1,\pm1}\rangle)/\sqrt{2}$ |
| 11 | 2 | $1_-$ | + | $2\hbar(\bar{\omega}+\delta/6)$ | $(g_1g_2-f_2^2)\Upsilon-f_2^2$ | $-3(13+2\Upsilon+2\Upsilon^2)/100$ | $\Sigma_\pm\pm e^{\mp i\varphi}\lvert\phi_{1,0};\phi_{1,\pm1}\rangle/2+$perm. |
| 12 | 2 | $1_-$ | − | $2\hbar(\bar{\omega}+\delta/6)$ | $(g_1g_2+f_2^2)\Upsilon+f_2^2$ | −39/20 | $\Sigma_\pm\pm e^{\mp i\varphi}\lvert\phi_{1,0};\phi_{1,\pm1}\rangle/2-$perm. |
| 13 | 2 | $1_+$ | + | $2\hbar(\bar{\omega}+\delta/6)$ | $g_1g_2\Upsilon+f_2^2$ | $-3(27+5\Upsilon)/100$ | $\Sigma_\pm e^{\mp i\varphi}\lvert\phi_{1,0};\phi_{1,\pm1}\rangle/2+$perm. |
| 14 | 2 | $1_+$ | − | $2\hbar(\bar{\omega}+\delta/6)$ | $g_1g_2\Upsilon-f_2^2$ | $-3(27-19\Upsilon)/100$ | $\Sigma_\pm e^{\mp i\varphi}\lvert\phi_{1,0};\phi_{1,\pm1}\rangle/2+$perm. |
| 15 | 2 | 0 | + | $2\hbar(\bar{\omega}+2\delta/3)$ | $g_2^2\Upsilon$ | $-3(34-14\Upsilon-\Upsilon^2)/100$ | $\lvert\phi_{1,0};\phi_{1,0}\rangle$ |

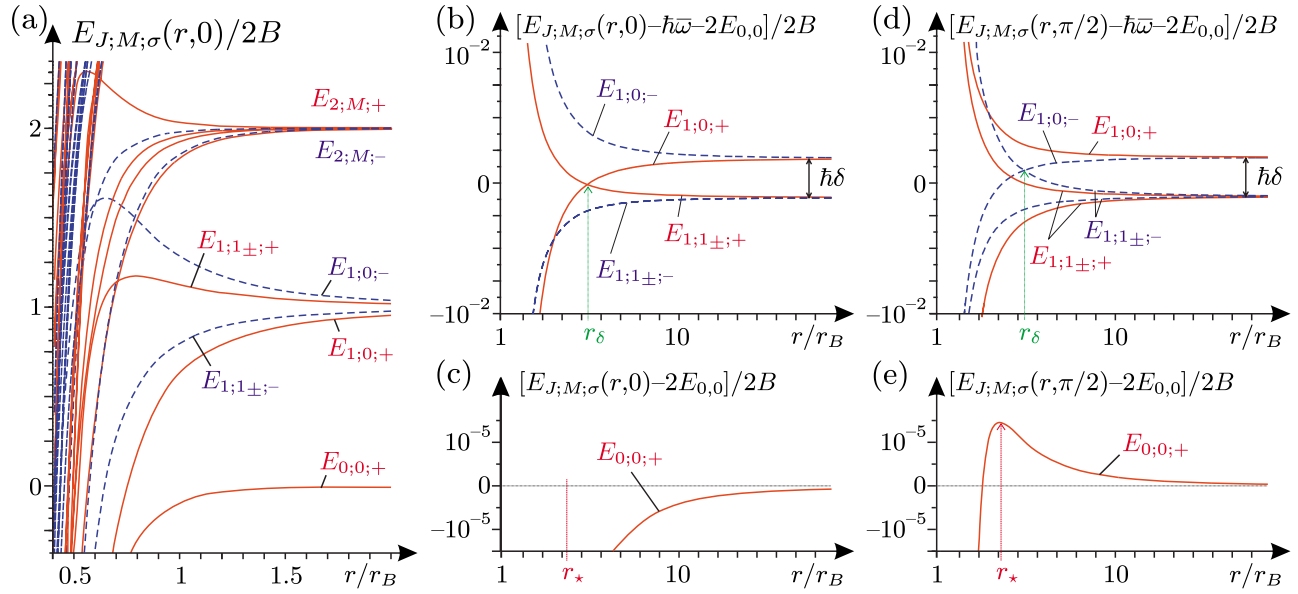


FIG. 6. (Color online) BO potentials $E_{J;M;\sigma}(r,\vartheta)$ for two molecules colliding in the presence of a dc field, with $\beta \equiv dE_{\rm dc}/B = 1/5$ and $(J;M;\sigma)$ the quantum numbers of Table III. The solid and dashed curves correspond to symmetric $(\sigma=+)$ and antisymmetric $(\sigma=-)$ eigenstates, respectively. (a) BO potentials for the 16 lowest-energy eigenstates $E_n(r,\vartheta=0)$. The molecular-core region is identified as the region $r<r_B=(d^2/B)^{1/3}$, while for $r\gg r_B$ the eigenstates group into manifolds separated by one quantum of rotational excitation $2B$. (b), (d) Blowups of the first excited energy manifold of (a) in the region $r\gtrsim r_B$ for $\vartheta=0$ and $\pi/2$, respectively. Note the electric-field-induced splitting $\hbar\delta \equiv 3B\beta^2/20$ (see Sec. II B 1). The distance $r_\delta$ where the dipole-dipole interaction becomes comparable to $\hbar\delta$ is $r_\delta=(d^2/\hbar\delta)^{1/3}$. (c), (e) Blowups of the ground-state potential $E_{0,0;+}(r,\vartheta)$ of (a) in the region $r\gtrsim r_B$ for $\vartheta=0$ and $\pi/2$, respectively. The distance $r_\star$ [cf. Eq. (22)], where the dipole-dipole interaction becomes comparable to the van der Waals attraction is indicated. Note the attractive (repulsive) character of the potential for $\vartheta=0$ $(\vartheta=\pi/2)$ and $r>r_\star$.

and van der Waals interactions become comparable. The height of this maximum is

$$V_\star = \frac{C_{3;0}^2}{4|C_{6;0}|} \approx \frac{B\beta^4}{54}, \tag{23}$$

and the curvature along $z$ is

$$\partial_z^2 V(r=r_\star, z=0) = -6C_{3;0}/r_\star^5 \equiv -m\omega_c^2/2,$$

which defines a characteristic frequency

$$\omega_c \equiv \left(\frac{12C_{3;0}}{mr_\star^5}\right)^{1/2}, \tag{24}$$

to be used below. The latter has a strong dependence $\beta^{8/3} = (dE_{\rm dc}/B)^{8/3}$ on the applied electric field.

We notice that if it were possible to confine the collisional dynamics to the $z=0$ plane, purely repulsive long-range interactions with a characteristic dipolar spatial dependence $\sim 1/r^3$ could be attained. In the following sections, we analyze the conditions for realizing sufficiently strong confinements to the $z=0$ plane by employing a tight harmonic optical trap in the $z$ direction.

Figure 6 shows the eigenvalues $E_n(\mathbf{r})$ as a function of the interparticle distance $r$, for $\beta=1/5$. The vector $\mathbf{r}$ is expressed in spherical coordinates $\mathbf{r}=(r,\vartheta,\phi)$, with $z=r\cos\vartheta$. Figure 6(a) shows the different behavior of the energy spectrum for $r<r_B$ and $r>r_B$, analogous to the zero-field case. Even at finite $\beta$ we can clearly distinguish the molecular core region $r<r_B$ where the adiabatic approximation breaks down. Figures 6(b)–6(e) are blowups of the two lowest-energy manifolds of Fig. 6(a), for $\vartheta=0$ and $\pi/2$, respectively. Unlike in the zero-field case, Figs. 6(b) and 6(d) show that the excited-state manifold with one quantum of rotation $(J_1+J_2=1)$ is asymptotically split into two submanifolds. This separation corresponds to the electric-field-induced splitting of the $J_j=1$ manifold of each molecule, and it is thus given by $\hbar\delta = 3B\beta^2/20$ of Eq. (5). More importantly, Figs. 6(c) and 6(e) show that the effective ground-state potential has a very different character for the cases $\vartheta=0$ and $\pi/2$. In fact, for $\vartheta=\pi/2$, corresponding to collisions in the $z=0$ plane [see Fig. 6(e)], the potential is repulsive and decaying at large distances as $1/r^3$ in agreement with the discussion above. On the other hand, for $\vartheta=0$ [see Fig. 6(c)] the potential is purely attractive, with dipolar character. As mentioned above, in the next section we show that the probability of sampling this attractive part of the potential during the collision can be largely suppressed in the case $\omega_\perp \neq 0$, for a sufficiently tight transverse trapping.

### 3. Parabolic confinement

The presence of a finite trapping potential of frequency $\omega_\perp$ in the $z$ direction provides for a position-dependent energy shift of Eq. (21). The new potential reads

$$V(\mathbf{r}) \equiv V_{\rm eff}^{\rm 3D}(\mathbf{r}) + \frac{1}{4}m\omega_\perp^2 z^2 = \frac{C_{3;0}}{r^3}(1-3\cos^2\vartheta) + \frac{C_{6;0}}{r^6} + \frac{1}{4}m\omega_\perp^2 z^2. \tag{25}$$

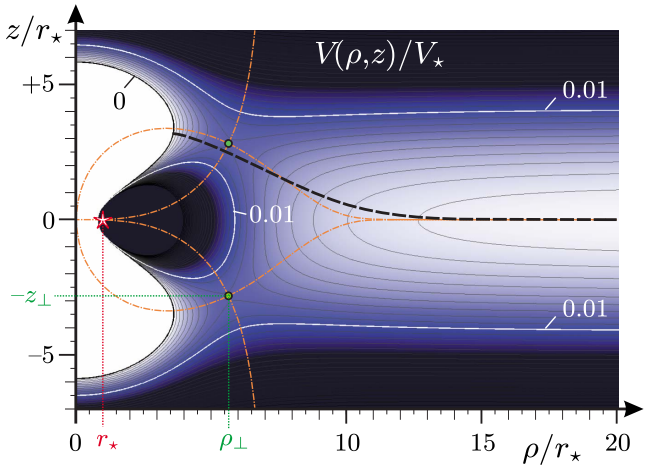


FIG. 7. (Color online) Contour plot of the effective potential $V(\rho,z)$ of Eq. (25), for two polar molecules interacting in the presence of a dc field $\beta>0$, and a confining harmonic potential in the $z$ direction, with trapping frequency $\omega_\perp=\omega_c/10$, where $\omega_c \equiv (12C_{3;0}/mr_\star^5)^{1/2}$ of Eq. (24) and $r_\star=(2|C_{6;0}|/C_{3;0})^{1/3}$ of Eq. (22). The contour lines are shown for $V(\rho,z)/V_\star \geq 0$, with $V_\star=B\beta^4/54$. Darker regions represent stronger repulsive interactions. The combination of the dipole-dipole interactions induced by the dc field and the harmonic confinement leads to realization of a 3D repulsive potential. The repulsion due to the dipole-dipole interaction and the harmonic confinement is distinguishable at $z\sim 0$ and $z/r_\star \sim \pm 7$, respectively. Two saddle points (circles) located at $(\rho_\perp, \pm z_\perp)$ separate the long-distance region where the potential is repulsive $\sim 1/r^3$ from the attractive short-distance region. The gradients of the potential are indicated by dash-dotted lines. The thick dashed line indicates the instanton solution for the tunneling through the potential barrier.

As noted before, for $z=0$ the repulsive dipole-dipole interaction dominates over the attractive van der Waals interaction at distances $r \gg r_\star$ given in Eq. (22). In addition, for $\omega_\perp>0$ the harmonic potential confines the particle's motion in the $z$ direction. Thus, the combination of the dipole-dipole interaction and the harmonic confinement yields a repulsive potential which provides for a three-dimensional barrier separating the long-distance from the short-distance regime. If the collisional energy is much smaller than this barrier, the particle's motion is confined to the long-distance region, where the potential is purely repulsive.

Figure 7 is a contour plot of $V(\mathbf{r})$ in units of $V_\star$ [cf. Eq. (23)], for $\beta>0$ and $\omega_\perp=\omega_c/10$, with $\mathbf{r}\equiv(\rho,z)=r(\sin\vartheta,\cos\vartheta)$ (the angle $\varphi$ is neglected due to the cylindrical symmetry of the problem). Darker regions correspond to a stronger repulsive potential. The repulsion due to the dipole-dipole and harmonic potentials is clearly distinguishable at $|z|/r_\star \sim 0$ and 7, respectively. The less-dark regions located at $(\rho_\perp, \pm z_\perp)\equiv \ell_\perp(\sin\vartheta_\perp, \pm\cos\vartheta_\perp)$ correspond to the existence of two saddle points (see the circles in Fig. 7). Here, $\ell_\perp$ and $\cos\vartheta_\perp$ are $\ell_\perp=(12C_{3;0}/m\omega_\perp^2)^{1/5}$ and $\cos\vartheta_\perp=\sqrt{1-(r_\star/\ell_\perp)^3}/\sqrt{5}$, respectively, while the barrier at the saddle point is $V(\rho_\perp, \pm z_\perp)=C_{3;0}/\ell_\perp^3+C_{6;0}/\ell_\perp^6$. The figure shows that for distances $r\gg \ell_\perp \geq r_\star, r_B$ the effective interaction potential Eq. (25) is purely repulsive. The existence of two saddle points at distances $r\sim\ell_\perp$ separating the long-from the short-distance regimes is a general feature of systems with $\beta>0$ and $\omega_\perp/\omega_c<1$. Thus, $\ell_\perp$ defines the characteristic length scale for attaining purely repulsive 3D potentials in the presence of a static electric field. Actually, we show below that for collisional energies smaller than $V(\rho_\perp, |z_\perp|)$ the dynamics of the particle can be reduced to a *quasi*-two-dimensional one, by tracing over the fast particle motion in the $z$ direction.

For strong trapping $\omega_\perp \geq \omega_c$, the two saddle points collapse into a single one located at $z=0$, and $\rho=\ell_\perp \sim r_\star$. In this limit the dynamics is purely 2D, with the particles strictly confined to the $z=0$ plane. The long-distance regime is separated from the short-distance one by a potential barrier of height $V(\ell_\perp,0)=V_\star=B\beta^4/54$. The amount of harmonic confinement required to achieve this pure 2D regime increases rapidly with $\beta$ as $\omega_c \propto \beta^{8/3}$. While for a typical rotational constant $B/h\sim 5$ GHz and a weak dc field $\beta=1/10$, $\omega_c$ is of order of $\omega_c/2\pi\sim 10$ kHz, for a (reasonable) electric field $\beta=1/3$ we find $\omega_c/2\pi\sim 1$ MHz. This value of $\omega_c$ exceeds the tightest experimental optical traps $\omega_\perp^{\max}/2\pi\sim 150$ kHz. Thus, in general the dynamics should be considered quasi-2D.

When an ensemble of polar molecules is considered, inelastic collisions and three-body recombination may lead the system to a potential instability, associated with the attractive character of the dipole-dipole interaction [35,50,51]. In our discussion, this instability is associated with the population of the short-distance region $r<\ell_\perp$, which can be efficiently suppressed. In fact, for collisional energies smaller than the potential barrier $V(\rho_\perp, \pm z_\perp)$ the particles are mostly confined to the long-distance regime, where they scatter elastically. That is, when a cold ensemble of molecules is considered the barrier provides for the stability of the system by "shielding" the short-distance attractive part of the two-body potential. In this limit, residual losses are due to the tunneling through the potential barrier. In the next section we estimate the tunneling rate $\Gamma$ associated with this process, and we show that it can be efficiently suppressed for reasonable values of $\beta$ and $\omega_\perp$. Thus, it is possible to realize stable 2D configurations of strongly interacting polar molecules interacting *via* dipole-dipole interactions [31].

#### *4. Stability of long-range collisions*

In the following we calculate the rate $\Gamma=\Gamma_0 e^{-S_E/\hbar}$ of particle tunneling through the barrier $V(\rho_\perp, \pm z_\perp)$ using a semiclassical or instanton approach [52]. In particular, we focus on determining the quantity $S_E$, the Euclidean action of the semiclassical trajectory [52], which is responsible for the exponential suppression of the tunneling. The constant $\Gamma_0$ is related to the quantum fluctuations around the semiclassical trajectory, and its value is strongly system dependent. For the crystalline phase of Ref. [31] (see also Fig. 3), it is the collisional "attempt frequency," proportional to the characteristic phonon frequency $\Gamma_0 \sim \sqrt{C_{3;0}/ma^5}$, with $a$ the mean interparticle distance.

The relative motion of the two particles in the effective potential $V(\mathbf{r})$ of Eq. (25) is analogous to that of a single (fictitious) particle with reduced mass $m/2$, and dynamics determined by the Hamiltonian $H=\mathbf{p}^2/m+V(\mathbf{r})$. The associ-

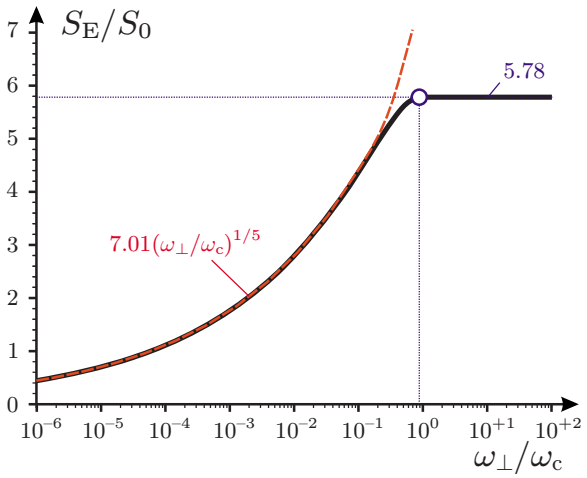


FIG. 8. (Color online) The Euclidean action $S_E$ of Eq. (28) as a function of $\omega_\perp/\omega_c$ (solid line). For $\omega_\perp<\omega_c'\approx 0.88\omega_c$ ($\omega_\perp>\omega_c'$) the bounce occurs for $z(0)\neq 0$ [within the plane $z(0)=0$]; see text. The point $\omega_c'$ is signaled by a circle. The dashed line is the $C_{6;0}$-independent expression $S_E\approx 7.01S_0(\omega_\perp/\omega_c)^{1/5}$ (see text), with $S_0=\sqrt{m|C_{6;0}|}/r_\star^2$. For $\omega_\perp>\omega_c'$ the action is $S_E\approx 5.78S_0$, which is $\omega_\perp$ independent, consistent with the bounce occurring in the $z=0$ plane.

ated Euclidean action, that is, the action in imaginary time $\tau$, is given by

$$S_E[\mathbf{r}(\tau)]=\int_{-\infty}^{+\infty}d\tau\left[\frac{m}{4}\left(\frac{\partial\mathbf{r}}{\partial\tau}\right)^2+V(\mathbf{r})\right], \tag{26}$$

where $\mathbf{r}(\tau)$ is the particle's trajectory. We remark that Eq. (26) corresponds to the action in real time, with an inverted potential $-V(\mathbf{r})$. The classical trajectories are found by minimizing the action Eq. (26), yielding the following equation of motion:

$$\frac{m}{2}\frac{d^2\mathbf{r}}{d\tau^2}=+\nabla V(\mathbf{r}). \tag{27}$$

The "energy" $\bar{E}=\mathbf{p}^2/m-V(\mathbf{r})$ is conserved along each classical trajectory. The instanton solution is then the trajectory with the smallest action $S_E$, which approaches $\mathbf{r}(\tau\to\pm\infty)=(\rho\to\infty,0)$ asymptotically at time $\tau\to\mp\infty$ (see the dashed line in Fig. 7). The energy of the particle along this trajectory is zero. The action $S_E$ reads

$$S_E=2\int_0^\infty d\tau\, 2V[\mathbf{r}(\tau)]=2\int_{\mathbf{r}(0)}^{\mathbf{r}(\infty)}ds\sqrt{mV(\mathbf{r})}, \tag{28}$$

where $\mathbf{r}(0)$ is the "bouncing point" reached at $\tau=0$ [52].

We solve Eq. (27) numerically for classical trajectories with zero energy, for generic values of $\beta$ and $\omega_\perp$. The obtained action $S_E$ is plotted in Fig. 8 as a function of $\omega_\perp/\omega_c$, in units of $S_0=\sqrt{m|C_{6;0}|}/r_\star^2=(2Bd^4m^3\beta^8/3^7)^{1/6}$. We notice that the action shows different behaviors for $\omega_\perp\ll\omega_c$ and $\omega_\perp\gg\omega_c$. In particular, for $\omega_\perp\ll\omega_c$ the action increases with increasing $\omega_\perp$, while for $\omega_\perp\gg\omega_c$ it is $\omega_\perp$ independent. The transition between the two different regimes mirrors the change in the nature of the underlying potential $V(\mathbf{r})$ as a function of $\omega_\perp/\omega_c$ described following Eq. (25), as explained below.

We find numerically that for $\omega<\omega_c'\approx 0.88\omega_c$ the bouncing point $\mathbf{r}(\tau=0)=[\rho(0),z(0)]$ of the instanton solution occurs for $z(0)\neq 0$ (see the dashed line in Fig. 7). This is consistent with the existence of two saddle points located at $V(\rho_\perp,\pm z_\perp)$, with $z_\perp>0$. Since the saddle points appear approximately at a length $r\sim\ell_\perp\gg r_\star$, it is expected that in this regime the action is independent of the short-distance behavior of the potential, that is, of the $C_{6;0}$ coefficient of the van der Waals attraction. Accordingly, Fig. 8 shows that $S_E$ is well approximated by $S_E\approx 7.01S_0(\omega_\perp/\omega_c)^{1/5}=5.86(C_{3;0}^2m^3\omega_\perp/8)^{1/5}=1.43\hbar(\ell_\perp/a_\perp)^2$ (dashed line), which depends only on the $C_{3;0}$ coefficient of the dipole-dipole interaction and the confinement along $z$, via $a_\perp=(\hbar/m\omega_\perp)^{1/2}$.

For $\omega\geq\omega_c'$ we find numerically that the bounce takes place in the plane $z=0$. This is consistent with the existence of a single saddle point located at $V(\ell_\perp,0)$ for $\omega_\perp>\omega_c$, as discussed in the previous section. The bouncing point is at $\rho(\tau=0)=\ell_\perp=r_\star/2^{1/3}$ and the action is $S_E=S_0 2^{5/3}\sqrt{\pi}\Gamma(7/6)/\Gamma(5/3)\approx 5.78S_0$. The latter is independent of $\omega_\perp$, which is again consistent with the collisional dynamics being purely 2D.

The reason why the transition between the two behaviors of the instanton solution happens at a value of $\omega_\perp$ that is slightly different from $\omega_c$ is that the instanton solution accounts for the kinetic energy of the fictitious particle. Thus, the particle is not always forced to follow the gradient of the potential [see the dash-dotted (red) lines in Fig. 7]. This results in the bounce occurring in the plane $z=0$ even for values of $\omega_\perp$ slightly smaller than $\omega_c$.

From the discussion above it follows that in the limit of strong interactions and tight transverse confinement $\Gamma$ rapidly tends to zero. We illustrate this for the example of SrO, which has a permanent dipole-moment of $d\approx 8.9$ D and mass $m=104$ amu. Then, for a tight transverse optical lattice with harmonic oscillator frequency $\omega_\perp=2\pi\times 150$ kHz and for a dc field $\beta=dE_{dc}/B=1/3$, we have $(C_{3;0}^2m^3\omega_\perp/8\hbar^5)^{1/5}\approx 3.39$ and obtain $\Gamma/\Gamma_0\approx e^{-5.86\times 3.39}\approx 2\times 10^{-9}$. Even for a dc field as weak as $\beta=dE_{dc}/B=1/6$, we still obtain a suppression by five orders of magnitude, as $\Gamma/\Gamma_0\approx e^{-5.86\times 1.94}\approx 10^{-5}$.

### 5. *Effective 2D interaction*

In the limit of strong interactions and tight optical confinement, it is possible to derive effective two-dimensional potentials by integrating out the fast particle motion in the transverse direction $z$.

For $r>\ell_\perp\gg a_\perp$, the two-particle eigenfunctions in the $z$ direction approximately factorize into products of single-particle harmonic oscillator wave functions $\psi_{k_1}(z_1)\psi_{k_2}(z_2)$. In first-order perturbation theory in $V_{\rm eff}^{2D}/\hbar\omega_\perp$, the effective 2D interaction potential $V_{\rm eff}^{2D}$ reads

$$V_{\rm eff}^{2D}(\boldsymbol{\rho})\approx\int dz_1dz_2\psi_0(z_1)^2\psi_0(z_2)^2V_{\rm eff}^{3D}(\mathbf{r})$$
$$=\frac{1}{\sqrt{2\pi}a_\perp}\int dz e^{-z^2/2a_\perp^2}V_{\rm eff}^{3D}(\mathbf{r}), \tag{29}$$

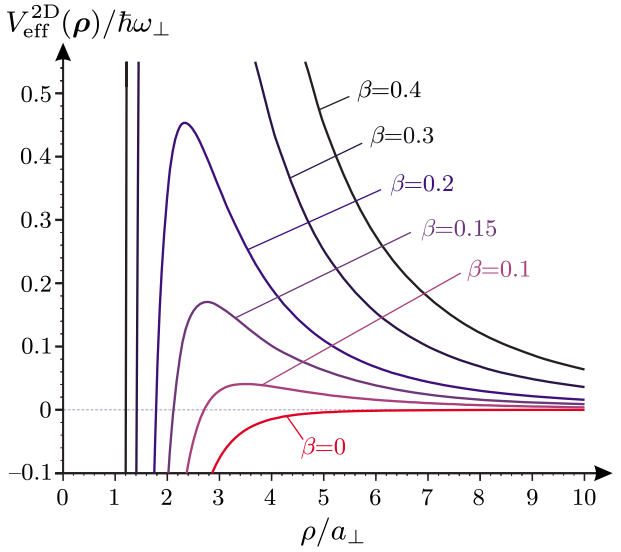


FIG. 9. (Color online) The ground-state effective 2D BO potentials $V_{\rm eff}^{\rm 2D}(\boldsymbol{\rho})$ of Eq. (29) as a function of the molecular separation $\rho$ in the $z=0$ plane for various strengths of the dc electric field $\beta=0,0.1,0.15,0.2,0.3,0.4$. The quantity $a_\perp$ is the harmonic oscillator length in the $z$ direction. The molecular parameters are chosen as $(d^4m^3B/\hbar^6)^{1/2}=1.26\times10^6$ and the frequency of the harmonic potential in the $z$ direction is $\omega_\perp=15B/10^6\hbar$. This corresponds to the case of SrO with a mass $m=104$ amu, a rotational constant $B\approx h\times10$ GHz, and a permanent dipole moment $d\approx8.9$ D in a tight confining potential with $\omega_\perp=2\pi\times150$ kHz, where $a_\perp\approx25$ nm.

and is shown in Fig. 9 for various strengths of the dc electric field, $\beta\equiv dE_{\rm dc}/B$. Expression Eq. (29) is valid for large separations $r>\ell_\perp\gg a_\perp$ where the potential is (much) smaller than the harmonic oscillator spacing, i.e., $|V_{\rm eff}^{\rm 2D}(\boldsymbol{\rho})|\ll\hbar\omega_\perp$. When this condition breaks down, more harmonic oscillator states should be considered in addition to the ground states $\psi_0(z_1)\psi_0(z_2)$ in deriving $V_{\rm eff}^{\rm 2D}$ from Eq. (21). In any case, for large separations $\rho\gg\ell_\perp$ the 2D potential reduces to

$$V_{\rm eff}^{\rm 2D}(\boldsymbol{\rho})\approx V_{\rm eff}^{\rm 3D}(\rho,0)=\frac{C_{3;0}}{\rho^3}+\frac{C_{6;0}}{\rho^6}.$$

Finally, in the adiabatic approximation we obtain the effective 2D Hamiltonian $H_{\rm eff}^{\rm 2D}$,

$$H_{\rm eff}^{\rm 2D}=\sum_{j=1}^{2}\frac{\bar{\mathbf{p}}_j^2}{2m}+V_{\rm eff}^{\rm 2D}(\boldsymbol{\rho}),\tag{30}$$

where $\bar{\mathbf{p}}_j\equiv(p_{x;j},p_{y;j})$ is the (two-dimensional) momentum in the plane $z=0$ of molecule $j=1,2$ and $\boldsymbol{\rho}\equiv(x_2-x_1,y_2-y_1)$ is the (two-dimensional) separation of the molecules in the plane $z=0$. The derivation of $H_{\rm eff}^{\rm 2D}$ is the central result of Sec. III A.

### B. Effective interactions in the presence of an ac microwave field

In this section we consider the interactions of two polar molecules in the presence of an ac microwave field of frequency $\omega$ and polarization $q$, with respect to the direction of transverse trapping $\mathbf{e}_z$, i.e., $\mathbf{E}_{\rm ac}(t)=E_{\rm ac}e^{-i\omega t}\mathbf{e}_q+$c.c. The spatial dependence of $\mathbf{E}_{\rm ac}(t)$ is neglected, in accordance with the discussion of Eq. (7). The field is blue detuned from the $J_j=0-1$ transition of the single-particle rotor spectrum by $\Delta=\omega-2B/\hbar>0$, with Rabi frequency

$$\Omega\equiv E_{{\rm ac}\,j}\langle1,q|d_{q;j}|0,0\rangle_j/\hbar=dE_{\rm ac}/\sqrt{3}\hbar.$$

The effects of the ac field on the two-particle scattering can be summarized as (a) inducing *oscillating* dipole-moments in each molecule, which determine long-range dipole-dipole interactions whose sign and angular dependence are given by the polarization $q$ and the orientation in space, $\mathbf{e}_r$; (b) inducing a coupling of the ground- and excited-state manifolds of the *two-particle* spectrum at a resonant (Condon) point $r_{\rm C}=(d^2/3h\Delta)^{1/3}$, where the dipole-dipole interaction becomes comparable to the detuning $\Delta$. This coupling is responsible for an avoided crossing, whose properties depend crucially on the polarization $q$. We show below that the character of the (3D) ground-state effective interaction potential is very different at distances larger and smaller than $r_{\rm C}$.

The basic features of the scattering in the presence of the ac field are depicted in Fig. 10. In the figure, the solid (dashed) lines are the bare ($E_{\rm ac}=0$) eigenvalues $E_{J;Y;\sigma}(\mathbf{r})$ of Eq. (20) for $\sigma=+$ ($\sigma=-$), plotted as a function of $r$. The color conventions are the same as in Fig. 5. The microwave field, which is detuned from the single-particle rotational spacing $2B$ by an amount $\hbar\Delta>0$, is represented by a black arrow. Analogous to Fig. 5, the excited-state manifold is split by the dipole-dipole interaction. This splitting has the effect of rendering the detuning position dependent, so that eventually the combined energy of the bare ground state plus a microwave photon becomes degenerate with the energies of some bare excited states. The resonant points are denoted as $r_{\rm C}$ and $r_{\rm C}'$ for the resonance with the two symmetric $|\Phi_{1;1_\pm;+}(\mathbf{r})\rangle\equiv[|\Phi_{1;+1;+}(\mathbf{r})\rangle\pm|\Phi_{1;-1;+}(\mathbf{r})\rangle]/\sqrt{2}$ and the antisymmetric state $|\Phi_{1;0;-}(\mathbf{r})\rangle$ respectively. The symmetric bare ground state is coupled by the ac field to the symmetric bare excited state $|\Phi_{1;1_-;+}(\mathbf{r})\rangle$ only, while the state $|\Phi_{1;1_+;+}(\mathbf{r})\rangle$ is dark. As explained below, this coupling induces a splitting of the field-dressed energy levels at $r_{\rm C}$. Due to this coupling, the 3D effective *dressed adiabatic* ground-state interaction potential inherits the character of the bare ground and excited potentials for $r\gg r_{\rm C}$ and $r\ll r_{\rm C}$, respectively (thick solid line in the figure). Since the symmetric excited-state potential is repulsive, during the collision the dynamics of the particle is confined to the region $r\geq r_{\rm C}$, that is, the ac coupling can determine an effective "shielding" of the inner part of the molecular interaction potentials (the molecular core of Fig. 5). This shielding is three dimensional and it is analogous to the optical shielding of Napolitano *et al.* developed in the context of ultracold atomic collisions [40,41]. In particular, we show below that the shielding efficiency depends strongly on the chosen polarization $q$ of the ac field (see Fig. 11 and text), a characteristic which was found both in theory and in experiments with cold atoms [40,42].

Analogous to the optical shielding case, one expects that diabatic couplings among symmetric states provide for a loss

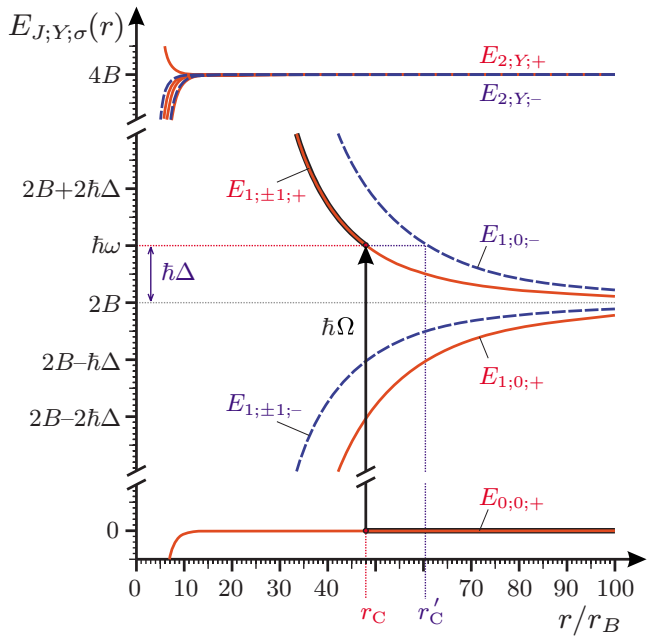


FIG. 10. (Color online) Schematic representation of the effects of an ac microwave field on the interaction of two molecules. The solid and dashed lines are the bare ($E_{ac}=0$) potentials $E_n(r) \equiv E_{J;Y;\sigma}(r)$ of Sec. III A 1 for the symmetric ($\sigma=+$) and antisymmetric ($\sigma=-$) states, respectively. An ac field of frequency $\omega=2B+\Delta$ is blue detuned by $\Delta=3B/10^6\hbar$ from the single-particle rotational spacing $2B$, with Rabi frequency $\Omega$. The dipole-dipole interaction splits the excited-state manifold, making the detuning position dependent. Eventually, the combined energy of the bare ground-state potential $E_{0;0;+}(r)$ and of an ac photon (vertical arrow) becomes degenerate with the energies of the bare symmetric $E_{1;\pm1;+}(r)$ and antisymmetric $E_{1;0;-}(r)$ potentials. The corresponding resonant points are denoted as $r_C=(d^2/3\hbar\Delta)^{1/3}$ (circles) and $r'_C=(2d^2/3\hbar\Delta)^{1/3}$, respectively. The resulting *dressed* ground-state potential is sketched by a thick solid line. For molecular parameters of SrO ($B\approx h\times 10$ GHz and $d\approx 8.9$ D) the detuning corresponds to $\Delta/2\pi=30$ kHz, and the lengths $r_B$ and $r_C$ are given by $r_B\approx 11$ nm and $r_C\approx 0.5$ $\mu$m, respectively.

mechanism in the 3D ground-state collision, for any finite collisional energies. In particular diabatic couplings, and therefore losses, are expected to be particularly relevant in the region $r\approx r_C$ and $r<r_C$, where the ground-state energy shows an avoided crossing with another potential, and the ground-state energy becomes doubly degenerate, respectively (see Figs. 10 and 11). When a harmonic confinement in the $z$ direction is considered, other loss channels may arise due to residual noncompensated tensor-shifts Eq. (12), coupling the ground state to the antisymmetric state $|\Phi_{1;0;-}(\mathbf{r})\rangle$, whose energy $E_{1;0;-}(\mathbf{r})$ crosses the ground-state potential at $r'_C=(2d^2/3\hbar\Delta)^{1/3}$ (see Fig. 10). When more particles are considered, three-body interactions are expected to generate similar couplings to the antisymmetric state. Three-body interactions are of concern since, as noted in Sec. I, we are interested in designing effective two-dimensional interaction potentials for pairs of molecules, which can lead to the realization of interesting phases for an ensemble of polar molecules in the *strongly interacting* regime (see Fig. 1 and Ref. [31]).

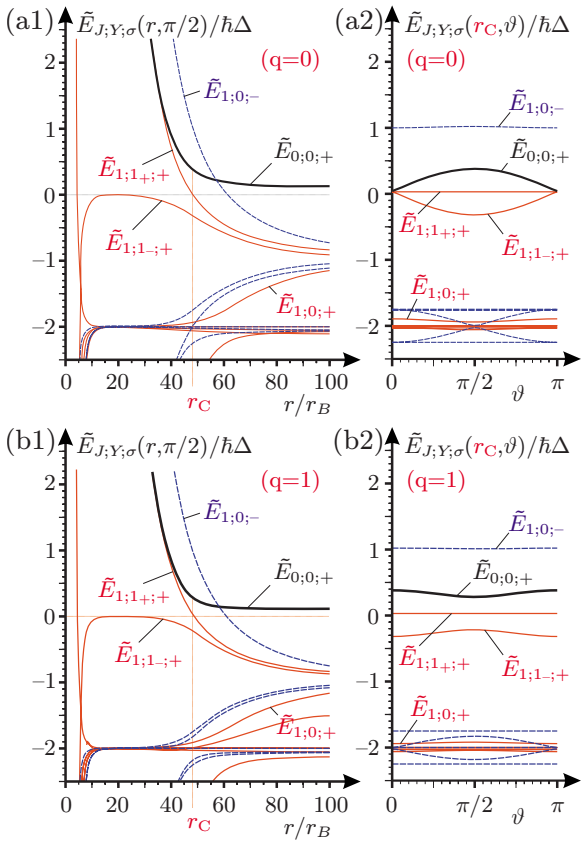


FIG. 11. (Color online) The dressed adiabatic potentials $\tilde{E}_n(r,\vartheta)$ of Eq. (37) for two molecules interacting in an ac field. The setup is the same as in Fig. 10. The field polarization is linear ($q=0$) in (a1) and (a2), while it is circular ($q=1$) in (b1) and (b2). The solid (red) and dashed (blue) lines correspond to the potentials for the symmetric ($\sigma=+$) and antisymmetric ($\sigma=-$) states, respectively. The thick continuous (black) line is the adiabatic dressed ground-state potential $\tilde{E}_{1;0;+}(r)$. (a1) and (b1) show the potentials as a function of the separation $r$ for interactions in the $z=0$ plane ($\vartheta=\pi/2$). The position of the resonant Condon point $r_C$ is indicated by a vertical line. (a2) and (b2) show the angular dependence of the potentials at $r=r_C$. Note that for $q=0$ (a2) $\tilde{E}_{0;0;+}(r)$ becomes degenerate with $\tilde{E}_{1;1_\pm;+}(r_C,\vartheta)$ at $\vartheta=0,\pi$, while it is nondegenerate at all angles for $q=1$ (b2), suggesting better shielding. The potential $\tilde{E}_{1;0;-}(r_C,\vartheta)$ has an energy larger than $\tilde{E}_{1;0;+}(r_C,\vartheta)$ for all angles $\vartheta$, indicating a level crossing ar $r>r_C$ (see text).

Because of all these loss mechanisms, *two-dimensional* shielding is not expected to be very efficient in the case of interactions in an ac field. However, in Sec. III C we show that most of these losses can be avoided, and an efficient 2D shielding recovered, by utilizing a properly chosen combination of static and microwave fields, and a tight harmonic confinement in the $z$-direction.

In the remainder of this section we further detail the interaction processes. This analysis is instrumental to the discussion of the collisions of two particles in the presence of both static and microwave fields, which is addressed in Sec. III C.

In Sec. III B 1 we derive the dressed adiabatic potentials for the interaction of two particles in an ac field. There, we

show that the shielding is strongly dependent on the chosen polarization of the ac field. In fact, for linear polarization ($q=0$) the width of the avoided crossing at the Condon point $r_C$ between the ground-state potential $E_{0;0;+}(\mathbf{r})$ and the potential $E_{1;+1;+}(\mathbf{r})$ is dependent on the value of the polar angle $\vartheta$, and it vanishes for $\vartheta=0$ and $\vartheta=\pi$. This vanishing of the width of the avoided crossing entails the existence of "holes" in the three-dimensional shielding, which allow for reaching the molecular-core region [see Figs. 11(a1) and 11(a2)]. On the other hand, for circular polarization ($q=1$) the potential is repulsive in three dimensions [see Figs. 11(b1) and 11(b2)]. Diabatic losses are most likely to occur at the Condon point $r_C$, and for $r<r_C$ due to couplings to the dark state $|\Phi_{1;1_+;+}(\mathbf{r})\rangle$, which becomes degenerate with the ground state. In Secs. III B 2 and III B 3, the interaction is further analyzed by deriving a perturbative expansion for the ground-state potential valid to second order in $\Omega/\Delta$, and by analyzing a reduced model Hamiltonian valid in the vicinity of $r_C$, respectively. There, it is argued that couplings to the antisymmetric manifold due to three-body interactions (and to the possible existence of residual tensor shifts for a harmonic confinement) reduce the efficiency of the shielding.

#### *1. Adiabatic potentials*

The total Hamiltonian for the collision of two particles in the presence of an ac field is

$$H(t)=\sum_{j=1}^{2}\left(\frac{\mathbf{p}_j^2}{2m}+\frac{1}{2}m\omega_\perp^2 z_j^2\right)+H_{\mathrm{int}}(\mathbf{r},t), \tag{31}$$

with

$$H_{\mathrm{int}}(\mathbf{r},t)=\sum_{j=1}^{2}\left[B\mathbf{J}_j^2-(E_{\mathrm{ac}}e^{-i\omega t}d_{q,j}+\mathrm{H.c.})\right]+V_{\mathrm{dd}}(\mathbf{r}). \tag{32}$$

Analogous to the discussion of Sec. III A, $H_{\mathrm{int}}(\mathbf{r},t)$ entirely determines the nontrivial dynamics of the system, since the harmonic motion of the center of mass is decoupled from the relative motion. The permutation symmetry $\sigma=\pm$ is conserved during the collision, since $H_{\mathrm{int}}(\mathbf{r},t)$ is invariant under the exchange of the positions of the two molecules $(j=1)\leftrightarrow(j=2)$, i.e., $\mathbf{r}\rightarrow-\mathbf{r}$. Thus, $H_{\mathrm{int}}(\mathbf{r},t)$, can be conveniently rewritten as $H_{\mathrm{int}}(\mathbf{r},t)=\Sigma_{\sigma=\pm}P_\sigma H_{\mathrm{int}}^{(\sigma)}(\mathbf{r},t)P_\sigma$, where $P_+$ and $P_-$ denote the projector onto the symmetric and antisymmetric manifolds, respectively.

We obtain the solution of the time-dependent problem is obtained analogously to Sec. II B 2 by diagonalizing the Hamiltonian $H_{\mathrm{int}}(\mathbf{r},t)$ in a Floquet picture and proceeds as follows. First we diagonalize the Hamiltonian in the absence of the ac field, $E_{\mathrm{ac}}=0$, as $H_{\mathrm{int}}(\mathbf{r})=\Sigma_n|\Phi_n(\mathbf{r})\rangle E_n(\mathbf{r})\langle\Phi_n(\mathbf{r})|$ with $n=(J;Y;\sigma)$, which is the same as Eq. (20), and in particular is *time independent* (see also Table II). Then, we consider the effect of the ac field, $\mathbf{E}_{\mathrm{ac}}(t)$ via a transformation to the Floquet picture, which is obtained by expanding the time-dependent wave function in a Fourier series in the ac frequency $\omega$. After applying the rotating wave approximation, i.e., keeping only the energy-conserving terms, we obtain the time-independent Hamiltonian $\tilde{H}(\mathbf{r})$, which describes the driven system. The Hamiltonian preserves the permutation symmetry, $\sigma=\pm$, i.e., $\tilde{H}_{\mathrm{int}}(\mathbf{r})=\Sigma_\sigma P_\sigma\tilde{H}_{\mathrm{int}}^{(\sigma)}(\mathbf{r})P_\sigma$. Analogously to the zero-field case of Sec. III A, we restrict the basis set to the 16 states belonging to the three lowest-energy manifolds. This is obtained by choosing a detuning much smaller than the rotational spacing $\Delta\ll B$, and working in the regime of weak saturation $\Omega\ll\Delta$. In fact, in this limit the anharmonicity of the single-particle rotational spectrum ensures that the population of high-energy rotational states is negligible. Finally, we solve for $\tilde{H}_{\mathrm{int}}(\mathbf{r})$ by diagonalizing the Hamiltonian in the symmetric and antisymmetric subspaces separately, e.g., $\tilde{H}_{\mathrm{int}}^{(\sigma)}(\mathbf{r})$.

The Hamiltonian $\tilde{H}_{\mathrm{int}}^{(+)}(\mathbf{r})$ for the symmetric subspace expressed in the basis $|\Phi_{J;Y;+}(\mathbf{r})\rangle$ with $(J;Y)=\{(0;0),(1;Y)|_{Y=-1,0,1},(2;Y)|_{Y=-2,-1,0_+,0_-,1,2}\}$ reads

$$\tilde{H}_{\mathrm{int}}^{(+)}(\mathbf{r})=-\hbar\left[\begin{array}{c|c|c|c|cc|cc|cc}
\Delta_{0;0}^{(+)} & \sqrt{2}\Omega_-^* & \sqrt{2}\Omega_0^* & \sqrt{2}\Omega_+^* & 0 & 0 & 0 & 0 & 0 & 0\\
\hline
\sqrt{2}\Omega_- & \Delta_{1;-1}^{(+)} & 0 & 0 & \sqrt{2}\Omega_-^* & \Omega_0^* & c_+\Omega_+^* & -c_-\Omega_+^* & 0 & 0\\
\sqrt{2}\Omega_0 & 0 & \Delta_{1;0}^{(+)} & 0 & 0 & \Omega_-^* & c_-\sqrt{2}\Omega_0^* & c_+\sqrt{2}\Omega_0^* & \Omega_+^* & 0\\
\sqrt{2}\Omega_+ & 0 & 0 & \Delta_{1;+1}^{(+)} & 0 & 0 & c_+\Omega_-^* & -c_-\Omega_-^* & \Omega_0^* & \sqrt{2}\Omega_+^*\\
\hline
0 & \sqrt{2}\Omega_- & 0 & 0 & \Delta_{2;-2}^{(+)} & 0 & 0 & 0 & 0 & 0\\
0 & \Omega_0 & \Omega_- & 0 & 0 & \Delta_{2;-1}^{(+)} & 0 & 0 & 0 & 0\\
0 & c_+\Omega_+ & \sqrt{2}c_-\Omega_0 & c_+\Omega_- & 0 & 0 & \Delta_{2;0_+}^{(+)} & 0 & 0 & 0\\
0 & -c_-\Omega_+ & \sqrt{2}c_+\Omega_0 & -c_-\Omega_- & 0 & 0 & 0 & \Delta_{2;0_-}^{(+)} & 0 & 0\\
0 & 0 & \Omega_+ & \Omega_0 & 0 & 0 & 0 & 0 & \Delta_{2;+1}^{(+)} & 0\\
0 & 0 & 0 & \sqrt{2}\Omega_+ & 0 & 0 & 0 & 0 & 0 & \Delta_{2;+2}^{(+)}
\end{array}\right]. \tag{33}$$

The Hamiltonian $\tilde{H}_{\rm int}^{(-)}(\mathbf{r})$ for the antisymmetric subspace on the basis $|\Phi_{J;Y;-}(\mathbf{r})\rangle$ with $(J;Y)=\{(1;Y)|_{Y=-1,0,1},(2;Y)|_{Y=-1,0,1}\}$ reads

$$\tilde{H}_{\rm int}^{(-)}(\mathbf{r})=-\hbar\left[\begin{array}{ccc|ccc} \Delta_{1;-1}^{(-)} & 0 & 0 & -\Omega_0^* & -\Omega_+^* & 0 \\ 0 & \Delta_{1;0}^{(-)} & 0 & \Omega_-^* & 0 & -\Omega_+^* \\ 0 & 0 & \Delta_{1;+1}^{(-)} & 0 & \Omega_-^* & \Omega_0^* \\ \hline -\Omega_0 & \Omega_- & 0 & \Delta_{2,-1}^{(-)} & 0 & 0 \\ -\Omega_+ & 0 & \Omega_- & 0 & \Delta_{2,0}^{(-)} & 0 \\ 0 & -\Omega_+ & \Omega_0 & 0 & 0 & \Delta_{2,+1}^{(-)} \end{array}\right]. \tag{34}$$

In Eqs. (33) and (34) off-resonant couplings of order $O(\Omega d^2/r^3B)$ between the various $J$ manifolds have been neglected. The detunings $\Delta_{J;Y}^{(\sigma)}$ and couplings $\Omega_Y$ in Eqs. (33) and (34) depend on the separation $\mathbf{r}$ of the two molecules as

$$\Delta_{J;Y}^{(\sigma)}\equiv\Delta_{J;Y}^{(\sigma)}(r)=J\omega-E_{J;Y;\sigma}(r)/\hbar, \tag{35}$$

$$\Omega_Y\equiv\Omega_Y(\vartheta,\varphi)=\Omega D_{q,Y}^1(\varphi,\vartheta,0)^*. \tag{36}$$

Here $D_{q,Y}^1(\varphi,\vartheta,0)\equiv\langle 1,q|\exp(-i\varphi J_z)\exp(-i\vartheta J_y)|1,Y\rangle$ are matrix elements of the rotation operator, which rotates the laboratory frame onto the frame where the collision axis is fixed along $\mathbf{e}_0$. The coefficients $c_\pm$ are $c_\pm=[(1\pm 1/\sqrt{3})/2]^{1/2}$.

As said above, a set of dressed BO potentials $\tilde{E}_n(\mathbf{r})$ and of adiabatic eigenstates $|\tilde{\Phi}_n(\mathbf{r})\rangle$ is obtained by diagonalizing the Hamiltonian $\tilde{H}_{\rm int}$ as

$$\tilde{H}_{\rm int}(\mathbf{r})=\sum_n|\tilde{\Phi}_n(\mathbf{r})\rangle\tilde{E}_n(\mathbf{r})\langle\tilde{\Phi}_n(\mathbf{r})|, \tag{37}$$

with $n=(J;Y;\sigma)$. The tilde refers to the implicit dependence of the dressed potentials and eigenstates on the Rabi frequency $\Omega$, the polarization $q$, and the detuning $\Delta$ of the external ac field. As mentioned above, we focus on blue detunings $\Delta=\omega-2B/\hbar>0$, since we are interested in repulsive potentials which can "shield" the short-range molecular-core interaction.

#### 2. Asymptotic expansion: $r\gg r_{\rm C}$

An insight into the nature of the dressed ground state potential can be obtained by deriving an expression for $\tilde{E}_0(\mathbf{r})\equiv\tilde{E}_{0;0;+}(\mathbf{r})$ perturbatively in the small parameter $\Omega/\Delta$. The perturbative expansion is valid at separations $r\gg r_{\rm C}\equiv(d^2/\hbar\Delta)^{1/3}$, where the dipole-dipole interaction in the first excited manifold $n=(1;Y;\sigma)$ is smaller than the detuning of the ac field. Then, to second order in $\Omega/\Delta$, the dressed ground-state potential reads

$$\begin{aligned}\tilde{E}_0(\mathbf{r})&\approx-\hbar\Delta_{0;0}^{(+)}(r)+\hbar\sum_{Y=-1}^{+1}\frac{2|\Omega_Y(\vartheta,\varphi)|^2}{\Delta_{1;Y}^{(+)}(r)-\Delta_{0;0}^{(+)}(r)}\\&\approx+\frac{2\hbar|\Omega|^2}{\Delta}-\frac{|\Omega|^2}{\Delta^2}\frac{d^2(2-3q^2)}{3r^3}(1-3\cos^2\vartheta),\end{aligned} \tag{38}$$

where terms of order $O(1/r^6)$ have been neglected. The first term in Eq. (38) describes a quadratic single-molecule ac Stark shift, which is positive for blue detunings. The second term is understood as follows. The ac field induces in each molecule an oscillating dipole moment of magnitude $\langle\mathbf{d}_j\rangle\sim d\Omega\,\mathbf{e}_q/\Delta$, and on average the oscillating dipoles give rise to an effective dipole-dipole interaction in the ground state, which is proportional to $\langle\mathbf{d}_j\rangle^2/r^3$. Equation (38) shows that the overall sign of the induced interaction can be changed by varying the polarization $q$.

The perturbative expression for the ground-state potential breaks down at $r\sim r_{\rm C}=(d^2/3\hbar\Delta)^{1/3}$, where two of the bare $J=1$ excited potentials $[E_{1;\pm1;+}(\mathbf{r})]$ become degenerate with the energy of the ground state plus a photon of frequency $\omega$.

While the validity of perturbation theory ceases at $r\sim r_{\rm C}$, further insight into the solution of the adiabatic scattering problem can be obtained by direct inspection of a specific example. Figure 11 shows the dressed BO potentials $\tilde{E}_n(\mathbf{r})$ of Eq. (37) for $\Delta=3B/10^6\hbar$ and $\Omega=\Delta/4$. The polarization is linear, $q=0$, in Figs. 11(a1) and 11(a2), while it is circular in Figs. 11(b1) and 11(b2), with $q=+1$. Figures 11(b2) and 11(b2) show $\tilde{E}_n(\mathbf{r})$ as a function of the separation $r$ for collisions in the plane $\vartheta=\arccos(z/r)=\pi/2$. Figures 11(a2) and 11(b2) depict the angular dependence of $\tilde{E}_n(\mathbf{r})$ at the Condon point $r=r_{\rm C}$ for the two polarizations $q=0$ and 1, respectively. In all the panels, the solid and dashed lines denote symmetric and antisymmetric potentials, respectively, while the dressed ground-state potential $\tilde{E}_0(\mathbf{r})=\tilde{E}_{0;0;+}(\mathbf{r})$ is represented by a thick solid line. Since we are interested in ground-state collisions, the figure suggests the two following observations. First, while the potential $\tilde{E}_0(\mathbf{r})$ is strongly repulsive for $r<r_{\rm C}$ and $\vartheta=\pi/2$, for both $q=0$ and 1 [Figs. 11(a1) and 11(b1)], the angular dependence at $r=r_{\rm C}$ is very different [Figs. 11(a2) and 11(b2)]. In particular, Fig. 11(a2) shows that for $q=0$ the repulsive potential is a maximum at $\vartheta=\pi/2$, while it vanishes at $\vartheta=0$ and $\pi$. This vanishing of the repulsion allows for the molecules to approach the molecular-core region, and thus the polarization $q=0$ does not provide for an efficient three-dimensional shielding of the molecular-core region. On the other hand, Fig. 11(b2) shows that the shielding may in principle work for $q=1$, since the ground-state potential is repulsive for any angle. The second observation is that a level crossing of the ground-state potential with the antisymmetric potential $\tilde{E}_{1,0,-}(\mathbf{r})$ appears at $r_{\rm C}'=2^{1/3}r_{\rm C}$ for all polarizations [Figs. 11(a1) and 11(b1)]. Couplings to this state can arise due to noncompensated residual tensor shifts, when a harmonic confinement in the $z$ direction is considered, or due to three-body interactions, when an ensemble of polar molecules is

considered. These couplings will induce losses in the ground-state interaction. In Sec. III C we show that the position of this level crossing can be shifted to distances $r \ll r_C$, and the associated losses can be avoided, by superimposing a weak static electric field onto the ac field. In this way, an efficient (2D) shielding of the molecular-core region can be recovered.

#### 3. Resonant Condon point: $r \sim r_C$

In the remainder of this section we analyze further the scattering process at the resonance point $r_C$. We restrict the discussion to the three relevant states $\{|\Phi_{0;0;+}(\mathbf{r})\rangle, |\Phi_{1;-1;+}(\mathbf{r})\rangle, |\Phi_{1;+1;+}(\mathbf{r})\rangle\}$, since all other symmetric states of the $J=1$ manifold are detuned by $\Delta_{J;\gamma}^{(\sigma)}(r) \geq \Delta \gg \Omega$. In this subspace the Hamiltonian Eq. (33) reads

$$\tilde{H}_{\mathrm{int}}(\mathbf{r}) = -\hbar \begin{bmatrix} \Delta_{0;0}^{(+)}(r) & \sqrt{2}\Omega_-(\vartheta,\varphi)^* & \sqrt{2}\Omega_+(\vartheta,\varphi)^* \\ \sqrt{2}\Omega_-(\vartheta,\varphi) & \Delta_{1;-1}^{(+)}(r) & 0 \\ \sqrt{2}\Omega_+(\vartheta,\varphi) & 0 & \Delta_{1;+1}^{(+)}(r) \end{bmatrix}. \tag{39}$$

For $q=0$ we have $\Omega_\pm(\vartheta,\varphi) = \pm\Omega \sin\vartheta/\sqrt{2}$ and the ground state couples only to the bright superposition state $[|\Phi_{1;-1;+}(\mathbf{r})\rangle - |\Phi_{1;+1;+}(\mathbf{r})\rangle]/\sqrt{2}$ with coupling $\sqrt{2}\hbar\Omega \sin\vartheta$. The orthogonal state $[|\Phi_{1;-1;+}(\mathbf{r})\rangle + |\Phi_{1;+1;+}(\mathbf{r})\rangle]/\sqrt{2}$ is dark with respect to the ac coupling. The dressed ground state is then a (position-dependent) superposition of bare ground and excited states and the corresponding dressed potential is

$$\tilde{E}_{0;0;+}(\mathbf{r})/\hbar = -\Delta_+(r) + \sqrt{\Delta_-(r)^2 + 2|\Omega|^2 \sin^2\vartheta}, \tag{40}$$

with $\Delta_\pm(r) \equiv [\Delta_{1;1}^{(+)}(r) \pm \Delta_{0;0}^{(+)}(r)]/2 \approx \Delta - d^2/3\hbar r^3$. We notice that for $q=0$ and $\vartheta=\pi/2$ the potential is repulsive with a $\sim 1/r^3$ radial dependence, due to the avoided crossing at $r=r_C$ [see Fig. 11(a1)]. For $\vartheta \neq \pi/2$ the splitting of the avoided crossing decreases as $\sin\vartheta$ and vanishes at $r=r_C$ for $\vartheta=0$ and $\vartheta=\pi$ [see Fig. 11(a2)]. Thus, close to the point $\mathbf{r}=r_C\mathbf{e}_0$, the molecules can penetrate the 3D shield provided by the ac field and approach the short-range molecular-core region, $r \ll r_C$. This behavior resembles that encountered in Sec. III A for the collision of two dipoles polarized by a dc field, when the intermolecular axis is parallel to the direction of the dc field [see Fig. 6(c)]. However, this unstable region now appears at distances $r \sim r_C \approx (d^2/3\hbar\Delta)^{1/3}$, which are larger than the short-distance length $r_B=(d^2/B)^{1/3}$ by a factor $\sim(B/\hbar\Delta)^{1/3}$. For a detuning on the order of tens of kilohertz and a rotational spacing of tens of gigahertz, $r_C$ is two orders of magnitude larger than $r_B$.

For a circularly polarized field $|q|=1$, we have $\Omega_\pm(\vartheta,\varphi) = \Omega e^{iq\varphi}(1 \pm q\cos\vartheta)/2$ and hence the ground-state couples to the bright superposition state $[\cos^2(\vartheta/2)|\Phi_{1;q;+}(\mathbf{r})\rangle + \sin^2(\vartheta/2)|\Phi_{1;-q;+}(\mathbf{r})\rangle]/\sqrt{(1+\cos^2\vartheta)/2}$ with an amplitude $\hbar|\Omega|\sqrt{1+\cos^2\vartheta}$, which is now nonvanishing for all angle $\vartheta$. The orthogonal superposition $[\cos^2(\vartheta/2)|\Phi_{1;-q;+}(\mathbf{r})\rangle - \sin^2(\vartheta/2)|\Phi_{1;q;+}(\mathbf{r})\rangle]\sqrt{(1+\cos^2\vartheta)/2}$ is dark with respect to the ac coupling. The dressed ground-state potential is

$$\tilde{E}_{0;0;+}(\mathbf{r})/\hbar = -\Delta_+(r) + \sqrt{\Delta_-(r)^2 + |\Omega|^2(1+\cos^2\vartheta)}, \tag{41}$$

with $\Delta_\pm(r)$ defined as in Eq. (40). The behavior of the ground-state potential in the $\vartheta=0$ plane is analogous to the linearly polarized case [see Figs. 11(a1) and 11(b1)]. However, in contrast to the $q=0$ case, now the width of the avoided crossing remains finite at all angles [see Fig 11(b2)], and the ac shielding of the molecular core is effective.

However, as noted above, the pure ac shielding mechanism has an intrinsic flaw that limits its utility, once an ensemble of polar molecules is considered. The antisymmetric state $|\Phi_{1;0;-}(\mathbf{r})\rangle$ is strongly repulsive with energy $-\hbar\Delta_{1;0}^{(-)}(r) \approx 2d^2/3r^3 - \hbar\Delta$ and thus gives rise to a real crossing at $r_C' = (2d^2/3\hbar\Delta)^{1/3} = 2^{1/3}r_C$ (see the dotted lines in Fig. 11). This crossing at distances *larger* than $r_C$ is expected to give rise to (strong) collisional losses when an ensemble of polar molecules is considered. In fact, three-body interactions can couple the ground state to the antisymmetric $|\Phi_{1;0;-}(\mathbf{r})\rangle$ state. In addition, analogous couplings can be provided by residual noncompensated tensor shifts, when a harmonic confinement in the $z$ direction is considered. In the next section we explain how some of these problems can be circumvented by introducing an additional static electric field. In that case, an efficient and collisionally stable 2D shielding of the inner part of the potential can be recovered.

### C. Effective interactions in the presence of both a dc and an ac field

In this section we consider the interactions of two polar molecules in the presence of both a weak dc field $\mathbf{E}_{\mathrm{dc}} = E_{\mathrm{dc}}\mathbf{e}_0$ with $\beta \equiv dE_{\mathrm{dc}}/B \ll 1$ and an ac microwave field $\mathbf{E}_{\mathrm{ac}}(t) = E_{\mathrm{ac}}e^{-i\omega t}\mathbf{e}_q + \mathrm{c.c.}$, where the polarization $q$ is defined with respect to the $z$-direction, $\omega$ is the frequency, $\Delta$ is the detuning from the single-particle resonance, and $\Omega$ is the Rabi frequency.

As explained in Sec. II B 1, the dc field partially splits the threefold degeneracy of the $J_j=1$ manifold of each molecule by an amount $\sim\hbar\delta = 3d^2E_{\mathrm{dc}}^2/20B$ (the modulus of the projection $|M|$ is conserved). When the ac field is superimposed on the weak dc field, this splitting can yield significative advantages regarding the stability of the ground-state collision. (a) The ground state can couple to a single nondegenerate excited state of the *two-particle* spectrum, thus avoiding diabatic losses due to the presence of symmetric (dark) states close to the ground state for $r \lesssim r_C \sim (d^2/3\hbar\Delta)^{1/3}$ (see the discussion in Sec. III B). In fact, because of the splitting $\hbar\delta$, the energies of other symmetric states become comparable to the dressed ground-state energy only at distances $r \sim r_\delta \equiv (d^2/\hbar\delta)^{1/3} \ll r_C$, where the dipole-dipole interaction becomes of the order of the splitting $\hbar\delta$. (b) The location $r_C'$ of the real crossing of Sec. III B is also shifted to small distances $r \lesssim r_\delta \ll r_C$, thus suppressing losses due to three-body-induced (or residual-tensor-shift-induced due to transverse confinement) couplings to the ground state.

Both of the outlined processes are shown in Figs. 12(a) and 12(b), which depict the bare ($E_{\mathrm{ac}}=0$) energy levels of the two-particle eigenstates with $J \leq 2$ as a function of the dis-

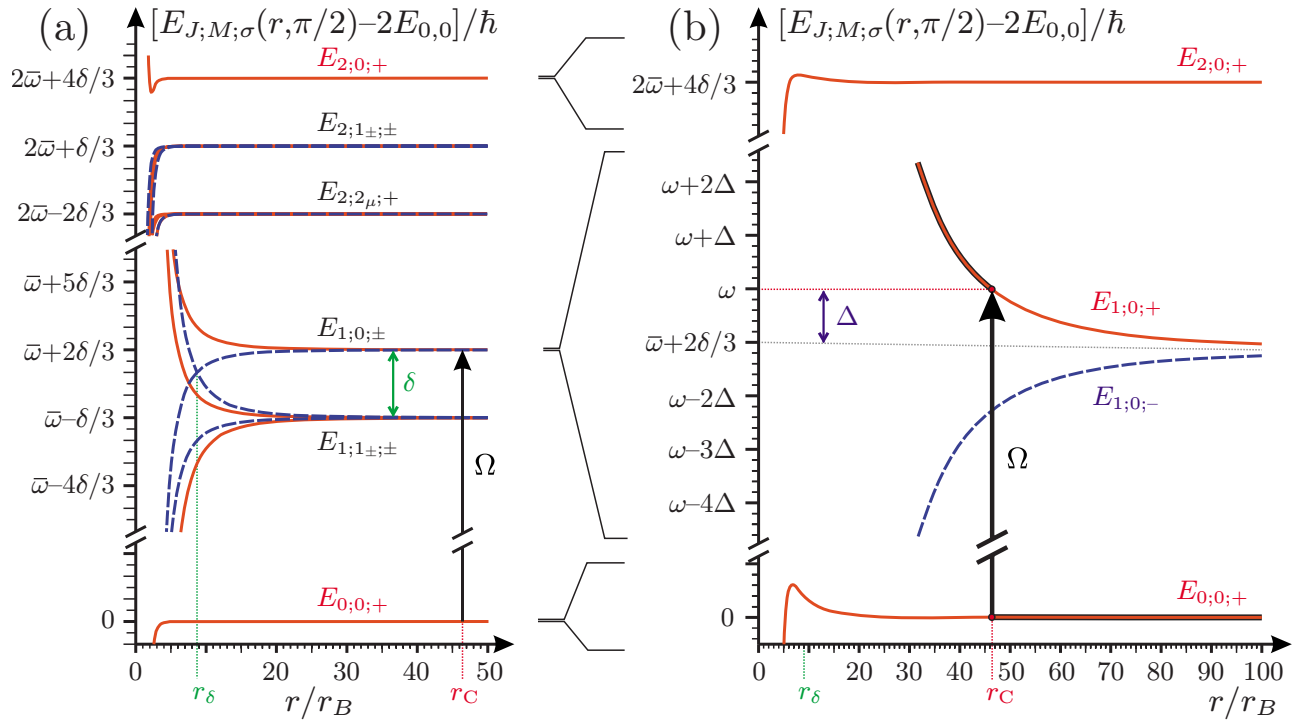


FIG. 12. (Color online) (a) Schematic representation of the effects of a dc and an ac microwave field on the interaction of two molecules. The solid and dashed lines are the bare potentials $E_n(\mathbf{r}) \equiv E_{J;M;\sigma}(r,\vartheta)$ of Sec. III A 2 with $\vartheta=\pi/2$ for interactions in the presence of the dc field only, for the symmetric ($\sigma=+$) and antisymmetric ($\sigma=-$) states, respectively. The dc field induces a splitting $\hbar\delta$ of the first excited manifold of the two-particle spectrum. A microwave field of frequency $\omega=\bar{\omega}+2\delta/3+\Delta$ is blue detuned by $\Delta>0$ from the single-particle rotational resonance. The dipole-dipole interaction further splits the excited-state manifold, making the detuning space dependent. Eventually, the combined energy of the bare ground-state potential $E_{0;0;+}(\mathbf{r})$ and an ac photon (black arrow) becomes degenerate with the energy of the bare symmetric $E_{1;0;+}(r,\pi/2)$. The resonant point $r_C=(d^2/3\hbar\Delta)^{1/3}$ occurs at $r\approx 46 r_B$. A second resonant Condon point occurs at (much) shorter distances $r_{C'}\lesssim r_\delta=(d^2/\hbar\delta)^{1/3}$ with an antisymmetric potential (not shown). (b) Blowup of the potentials of (a) with $M=0$ (see text in Sec. III C 2). The *dressed* ground-state potential is sketched by a thick solid line.

tance $r$, for $\beta=1/10$. The polarization of the ac field is $q=0$ and its frequency $\omega$ is blue detuned from the $|\phi_{0,0}\rangle \rightarrow |\phi_{1,0}\rangle$ transition of the single-particle spectrum by an amount $\Delta=\omega-(\bar{\omega}+2\delta/3)>0$. In the figure, the continuous (red) and dashed (blue) curves are the bare BO potentials for the symmetric and antisymmetric states, respectively. The presence of the ac field is signaled by a black arrow at the resonant (Condon) point $r_C\sim(d^2/3\hbar\Delta)^{1/3}$. Analogous to the case of Fig. 6(d), Fig. 12(a) shows that the $J=1$ manifold is asymptotically split by the dc Stark shift $\hbar\delta$. As said above, for $r\gg r_\delta$ this splitting suppresses the coupling among states of the $J=1$ manifold due to dipole-dipole interactions. Moreover, we note that, since the characteristic length $r_\delta$ is such that $r_\delta\ll r_C$ and $r'_C\lesssim r_\delta$ (not shown in the figure), the presence of the splitting ensures that $r_C\gg r'_C$, as opposed to the $E_{dc}=0$ case of Sec. III B. As a consequence, for $r\gg r_\delta>r'_C$ we expect diabatic and three-body-induced losses to be largely suppressed. Then, we show below that a strong optical confinement in the $z$ direction allows for the realization of stable 2D collision setups, as in Sec. III A. However, at variance with the dc case of Sec. III A, utilizing a combination of dc and ac fields allows for much greater flexibility in designing interparticle interactions. In particular, we here focus on the realization of a 2D potential achievable with a single ac field, whose character is very different at distances larger and smaller than $r_C$.

In the remainder of this section, we discuss further the above-mentioned processes. In Sec. III C 1 we derive the 3D dressed adiabatic potentials for interactions in the presence of combined dc and ac fields. In Secs. III C 2 and III C 3 we illustrate the main features of the two-particle interaction, by specializing to the case where the ac field polarization is linear ($q=0$), and by solving a model Hamiltonian comprising only a limited number of states, whose energies are close to that of the ground state. An expression for the ground-state interaction potential is obtained which shows that at large distances $r\gg r_C$ the potential has a behavior $\sim 1/r^3$ similar to that obtained for two molecules in a dc field. However, now the effective dipolar strength is given by the combination of both the dc *and* the ac fields, and it can be much weaker than for $r<r_C$. Thus, 3D interaction potentials can be engineered that have a marked steplike character, being strongly and weakly repulsive at distances smaller and larger than $r_C$, respectively. Analogously to the dc case of Sec. III A, an effective 2D interaction potential shielding of the short-range region $r\ll r_\delta\ll r_C$ is obtained by adding a harmonic confinement in the $z$ direction and tracing over the fast particle motion along $z$ (see Secs. III C 4 and III C 5).

### *1. Adiabatic potentials*

The total Hamiltonian including the couplings to dc and ac fields reads

$$H(t) = \sum_j \left( \frac{\mathbf{p}_j^2}{2m} + \frac{1}{2} m\omega_\perp^2 z_j^2 \right) + H_{\rm int}(\mathbf{r},t), \tag{42}$$

with

$$H_{\rm int}(\mathbf{r},t) = \sum_j [B\mathbf{J}_j^2 - E_{\rm dc} d_{0;j} - (E_{\rm ac} e^{-i\omega t} d_{q;j} + \text{H.c.})] + V_{\rm dd}(\mathbf{r}). \tag{43}$$

Similarly to the discussion following Eq. (18), the nontrivial system dynamics is determined by the dynamics of the relative degrees of freedom, which decouple from the harmonic motion of the center of mass. In this section we set $\omega_\perp = 0$ in Eq. (42), and thus diagonalizing the Hamiltonian for the relative coordinates in the adiabatic limit corresponds to diagonalizing $H_{\rm int}(\mathbf{r},t)$. The case $\omega_\perp \neq 0$ is treated in subsequent sections.

The Hamiltonian $H_{\rm int}(\mathbf{r},t)$ is invariant under the permutation of the two molecules, $(j=1) \leftrightarrow (j=2)$, and thus it can be conveniently rewritten as $H_{\rm int}(\mathbf{r},t) = \Sigma_{\sigma=\pm} P_\sigma H_{\rm int}^{(\sigma)}(\mathbf{r},t) P_\sigma$. Here $P_+$ and $P_-$ are the projectors onto the manifold of symmetric and antisymmetric states, respectively. Since (several) external fields are present, parity is not conserved.

In Sec. III A 2 we have already diagonalized $H_{\rm int}(\mathbf{r},t)$ in the absence of the ac field, that is $H_{\rm int}(\mathbf{r}) = \Sigma_n |\Phi_n(\mathbf{r})\rangle E_n(\mathbf{r}) \times \langle \Phi_n(\mathbf{r})|$. The corresponding adiabatic potentials $E_n(\mathbf{r})$ are shown in Fig. 6, together with the corresponding quantum numbers $n=(J;M;\sigma)$. We remark that $J$ is not a good quantum number since the electric field breaks the parity for each molecule; thus $J=J_1+J_2$ merely indicates the asymptotic manifold. The corresponding adiabatic potentials and eigenstates for the ground state $n=(0;0;+)$ [valid for $r \gg r_B = (d^2/B)^{1/3}$] and the lowest excited states [valid for $r \gg r_\delta = (d^2/\hbar\delta)^{1/3}$] are given in Table III. Our goal in this section is to extend that treatment to account for the driving by the ac microwave field, which we assume to be near resonant with the transition from the ground to the first excited manifold, i.e., $\omega \sim \bar{\omega} + (2/3 - q^2)\delta$ for polarizations $q=0,\pm 1$ (see Fig. 4). The average energy separation $\hbar\bar{\omega}$ is defined in Eq. (6).

Since for $\beta \lesssim 1$ the single-particle rotor spectrum is strongly anharmonic and the ac field is near resonant with the $J_j = 0 \leftrightarrow 1$ transition, we restrict our discussion to the rotor states with $J_j = 0,1$ for each molecule, that is, we consider 16 two-particle states. Moreover, we focus on the region $r \gg r_\delta$, where the dipole-dipole interaction is (much) weaker than the dc-field-induced splitting $\hbar\delta$ in the excited states. Therefore (up to corrections of order $\sim d^2/\hbar\delta r^3$ and $\sim d^2/Br^3$) the states $|\Phi_{J;M;\sigma}(\mathbf{r})\rangle$ are given by the states $|\Phi^{(0)}_{J;M;\sigma}(\vartheta,\varphi)\rangle \equiv |\Phi_{J;M_\mu;\sigma}(r\to\infty,\vartheta,\varphi)\rangle$, which are reported in Table III. These states are independent of $r$, that is, they depend only on the orientation of the two molecules. In analogy to the treatment of Sec. III B, we utilize the approximate states $|\Phi_{J;M;\sigma}(\mathbf{r})\rangle$to diagonalize the time-dependent Hamiltonian $H_{\rm int}(\mathbf{r},t)$ in a Floquet picture. We expand the time-dependent wave function in a Fourier series in the ac frequency $\omega$. After applying the rotating wave approximation, i.e., keeping only the energy-conserving terms, we obtain the time-independent Hamiltonian $\tilde{H}(\mathbf{r})$, which again preserves the permutation symmetry, $\sigma=\pm$. The Hamiltonian $\tilde{H}_{\rm int}^{(+)}(\mathbf{r})$ for the symmetric manifold $(\sigma=+)$ is expressed in the basis $\{|\Phi_{J;M_\mu;\sigma=+}(\mathbf{r})\rangle\}$ with

$$(J;M_\mu) = \{(0;0),(1;1_\mp)|;(1;0);(2;2_\mu)|_{\mu=-,0,+};(2;1_\mp);(2;0)\}$$

as

$$\tilde{H}_{\rm int}^{(+)}(\mathbf{r}) = -\hbar \left[\begin{array}{c|cc|c|ccc|cc|c} \Delta^{(+)}_{0;0} & \sqrt{2}\Omega_-^* & \sqrt{2}\Omega_+^* & \sqrt{2}\Omega_0^* & 0 & 0 & 0 & 0 & 0 & 0 \\ \hline \sqrt{2}\Omega_- & \Delta^{(+)}_{1;1_-} & 0 & 0 & \Omega_+^* & -c_+\Omega_-^* & c_-\Omega_-^* & \Omega_0^* & 0 & 0 \\ \sqrt{2}\Omega_+ & 0 & \Delta^{(+)}_{1;1_+} & 0 & \Omega_-^* & c_-\Omega_+^* & c_+\Omega_+^* & 0 & \Omega_0^* & 0 \\ \hline \sqrt{2}\Omega_0 & 0 & 0 & \Delta^{(+)}_{1;0} & 0 & 0 & 0 & \Omega_-^* & \Omega_+^* & \sqrt{2}\Omega_0^* \\ \hline 0 & \Omega_+ & \Omega_- & 0 & \Delta^{(+)}_{2;2_-} & 0 & 0 & 0 & 0 & 0 \\ 0 & -c_+\Omega_- & c_-\Omega_+ & 0 & 0 & \Delta^{(+)}_{2;2_0} & 0 & 0 & 0 & 0 \\ 0 & c_-\Omega_- & c_+\Omega_+ & 0 & 0 & 0 & \Delta^{(+)}_{2;2_+} & 0 & 0 & 0 \\ \hline 0 & \Omega_0 & 0 & \Omega_- & 0 & 0 & 0 & \Delta^{(+)}_{2;1_-} & 0 & 0 \\ 0 & 0 & \Omega_0 & \Omega_+ & 0 & 0 & 0 & 0 & \Delta^{(+)}_{2;1_+} & 0 \\ \hline 0 & 0 & 0 & \sqrt{2}\Omega_0 & 0 & 0 & 0 & 0 & 0 & \Delta^{(+)}_{2;0} \end{array}\right], \tag{44}$$

$\Delta^{(\sigma)}_{J;M_\mu} \equiv \Delta^{(\sigma)}_{J;M_\mu}(r,\vartheta) = J\omega - E_{J;M_\mu;\sigma}(r,\vartheta)/\hbar$ denote position-dependent detunings (for each rotational excitation), $\Omega_\pm \equiv \Omega_\pm(\varphi)$ are orientation-dependent couplings, which are detailed below, and $c_\pm \equiv c_\pm(\vartheta) = \cos(\xi/2) \pm \sin(\xi/2)$ depends on the polar angle $\vartheta$. The parameter $\xi$ is defined in the caption of Table III.

The Hamiltonian $\tilde{H}_{\rm int}^{(-)}(\mathbf{r})$ for the antisymmetric manifold $(\sigma=-)$ expressed in the basis $\{|\Phi_{J;M_\mu;\sigma=-}(\mathbf{r})\rangle\}$ with $(J;M_\mu) = \{(1;1_\mp);(1;0);(2;2);(2;1_\mp)\}$ reads

$$\tilde{H}_{\rm int}^{(-)}(\mathbf{r}) = -\hbar \left[\begin{array}{cc|c|cc|cc} \Delta_{1;1_-}^{(-)} & 0 & 0 & \Omega_+^* & \Omega_0^* & 0 \\ 0 & \Delta_{1;1_+}^{(-)} & 0 & -\Omega_-^* & 0 & \Omega_0^* \\ \hline 0 & 0 & \Delta_{1;0}^{(-)} & 0 & -\Omega_-^* & -\Omega_+^* \\ \hline \Omega_+ & -\Omega_- & 0 & \Delta_{2;2}^{(-)} & 0 & 0 \\ \hline \Omega_0 & 0 & -\Omega_- & 0 & \Delta_{2;1_-}^{(-)} & 0 \\ 0 & \Omega_0 & -\Omega_+ & 0 & 0 & \Delta_{2;1_+}^{(-)} \end{array}\right]. \tag{45}$$

In Eqs. (44) and (45) we neglected off-resonant (second-order) corrections $\sim\Omega_M(\varphi)d^2/\hbar\delta r^3$ to the Rabi frequency. The couplings $\Omega_-(\varphi),\Omega_0,\Omega_+(\varphi)$ are given by $\Omega_-(\varphi)=qf_1E_{\rm ac}e^{iq\varphi}/\sqrt{2}$, $\Omega_0=(1-q^2)f_0E_{\rm ac}$, $\Omega_+(\varphi)=qf_1E_{\rm ac}e^{iq\varphi}/\sqrt{2}$, respectively. Thus for linear polarization ($q=0$) one has $\Omega_0\equiv\Omega$ and $\Omega_\pm=0$, while for circular polarization ($|q|=1$) $\Omega_0=0$ and $\Omega_+(\varphi)=\pm\Omega_-(\varphi)=\Omega e^{\pm i\varphi}/\sqrt{2}$ for $q=\pm1$, respectively.

#### 2. Model Hamiltonian for $\Delta \ll \delta$

In the following we illustrate the main features of the scattering in the combined dc and ac fields, using the example of Fig. 12. The Rabi frequency $\Omega$ is chosen real and positive and in particular smaller than the detuning, $\Omega\ll\Delta$. Moreover, we choose $\Delta\ll\delta$ since we want to address the potentials in regions where the two molecules in the first excited two-particle manifold are aligned by the dc field and not by the dipole-dipole interaction (see Fig. 12). The figure shows that for $r\gg r_\delta$ the bare ($E_{\rm ac}=0$) states $|\Phi_{J;M;\sigma}(\mathbf{r})\rangle$ with $M\neq0$ are largely detuned from resonance by an amount of order $\delta\gg\Delta$. Thus, the discussion of Eqs. (44) and (45) can be simplified by restricting the Hilbert space to the four states with $M=0$ only. For our basis set, these are the three symmetric states $|\Phi_{J;0;+}(\mathbf{r})\rangle$ with $J=0,1,2$ and the antisymmetric state $|\Phi_{1;0;-}(\mathbf{r})\rangle$. Then, Eqs. (44) and (45) reduce to

$$\tilde{H}_{\rm int}^{(+)}(\mathbf{r}) = -\hbar \begin{bmatrix} \Delta_{0;0}^{(+)} & \sqrt{2}\Omega & 0 \\ \sqrt{2}\Omega & \Delta_{1;0}^{(+)} & \sqrt{2}\Omega \\ 0 & \sqrt{2}\Omega & \Delta_{2;0}^{(+)} \end{bmatrix}, \tag{46a}$$

$$\tilde{H}_{\rm int}^{(-)}(\mathbf{r}) = -\hbar[\Delta_{1,0}^{(-)}]. \tag{46b}$$

The position dependence of the detunings $\Delta_{J;0}^{(\sigma)}\equiv\Delta_{J;0}^{(\sigma)}(r,\vartheta)$ has the usual dipolar form $\Delta_{J;0}^{(\sigma)}(r,\vartheta)\sim\Upsilon/r^3$, with $\Upsilon\equiv1-3\cos^2\vartheta$. Explicitly, we have $\Delta_{J;0}^{(\sigma)}(r,\vartheta)=J\Delta-[C_{3;(J;0;\sigma)}\Upsilon/r^3-C_{6;(J;0;\sigma)}(\vartheta)/r^6]/\hbar$. The coefficients $C_{3;n}$ and $C_{6;n}(\vartheta)$ are given in Table III for $n=0,5,15$ (symmetric states) and $n=6$ (antisymmetric state), respectively. For the following discussion, it is important to notice that for a weak dc electric field $\beta\ll1$, the $C_{3;n}$ coefficients $C_{3;(0;0;+)}\equiv g_0^2\approx(d\beta/3)^2$ and $C_{3;(2;0;+)}\equiv g_2^2\approx(d\beta/5)^2$are quite small, since they are suppressed by a factor $\sim\beta^2$. On the other hand, the coefficients $C_{3;(1;0;\pm)}\equiv g_0g_2\pm f_1^2\approx\pm d^2/3$ for states belonging to the first excited manifold are as large as the bare dipolar coefficients (see Tables I and III).

By diagonalizing Eq. (46a) we obtain the three dressed symmetric potentials $\tilde{E}_{J;0;+}(\mathbf{r})$ (with $J=0,1,2$) in terms of complex cubic roots by

$$\tilde{E}_{J;0;+}(\mathbf{r}) = \hbar\sum_{\pm} e^{\pm2\pi iJ/3}\left(-\frac{Q}{2}\pm i\sqrt{\frac{P^3}{27}-\frac{Q^2}{4}}\right)^{1/3} - \hbar\bar{\Delta}(r,\vartheta), \tag{47}$$

where $P\equiv4\Omega^2+\Sigma_J[\Delta_{J;0}^{(+)}(r,\vartheta)-\bar{\Delta}(r,\vartheta)]^2/2$, $Q=2\Omega^2\times[\Delta_{1;0}^{(+)}(r,\vartheta)-\bar{\Delta}(r,\vartheta)]-\Pi_J[\Delta_{J;0}^{(+)}(r,\vartheta)-\bar{\Delta}(r,\vartheta)]$, and $\bar{\Delta}(r,\vartheta)=\Sigma_J\Delta_{J;0}^{(+)}(r,\vartheta)/3$. The dressed potential for the antisymmetric state, $\tilde{E}_{1;0;-}(\mathbf{r})=-\hbar\Delta_{1;0}^{(-)}(r,\vartheta)$, is the same as the bare one.

The dressed potentials $\tilde{E}_{J;0;\sigma}(r,\vartheta)$ are plotted in Fig. 13, for $\Delta=4\Omega=3B/10^6\hbar$, $B=h\times10$ GHz, linear polarization ($q=0$), and $\beta=1/10$. These parameters are the same as in Fig. 12. In particular, Fig. 13(a) shows $\tilde{E}_{J;0;\sigma}(r,\vartheta=\pi/2)$ as a function of the distance $r$, for molecules on the plane $z=r\cos\vartheta=0$ ($\vartheta=\pi/2$). Figure 13(b) is a three-dimensional representation of the potential-energy surfaces $\tilde{E}_{J;0;+}(r,\vartheta)\equiv\tilde{E}_{J;0;+}(\rho,z)$ for the three symmetric states $J=0,1,2$, for finite transverse displacements $z=r\cos\theta$ ($\vartheta\neq\pi/2$), while Fig. 13(c) is the same as Fig. 13(b), with the addition of the potential $\tilde{E}_{1;0;-}(\rho,z)$ for the antisymmetric state.

In Fig. 13(a) the dressed ground-state potential $\tilde{E}_{0;0;+}(r,\pi/2)$ is the thick solid curve with largest energy, which undergoes an avoided crossing with the potential $\tilde{E}_{1;0;+}(r,\pi/2)$ at a distance $r_C\sim(d^2/3\hbar\Delta)^{1/3}$. The precise value of $r_C$ is derived below. The figure shows that the Condon point $r_C$ separates an inner region $r<r_C$ where the ground-state potential is strongly repulsive, $\tilde{E}_{0;0;+}(r<r_C,\pi/2)\sim\tilde{C}_3(r<r_C)/r^3$, from an outer region $r>r_C$ where the potential is only weakly repulsive, $\tilde{E}_{0;0;+}(r>r_C,\pi/2)\sim\tilde{C}_3(r>r_C)/r^3$ with $\tilde{C}_3(r>r_C)\ll\tilde{C}_3(r<r_C)$.This marked dependence of the potential strength on $r$ is the realization of the steplike potential of Fig. 2, and it is due to the fact that the dressed ground state inherits the character of the bare ground state and of the bare state $|\Phi_{1;0;+}(\mathbf{r})\rangle$ for $r>r_C$ and $r<r_C$, respectively. Thus, we have $\tilde{C}_3(r>r_C)\sim C_{3;(0;0;+)}\approx(d\beta/3)^2$ and $\tilde{C}_3(r<r_C)\sim C_{3;(1;0;+)}\approx d^2/3$. A harmonic confinement in the $z$ direction will be added in Sec. III C 4 to ensure the stability of the 2D interaction.

Figure 13(b) is a three-dimensional representation of the dressed adiabatic potentials $\tilde{E}_{J;M;+}(\mathbf{r})$ for the symmetric states, plotted as a function of $\rho=r\sin\vartheta$ and $z=r\cos\vartheta$. Darker regions (in the online version: darker red/darker blue) correspond to stronger repulsive/attractive. The thin gray lines are equipotential energy contours. For $z=0$ ($\rho$ axis) we recognize the case of Fig. 13(a), where the symmetric ground-state potential has the largest energy. The position of the Condon point $r_C$ is indicated by an arrow. The avoided crossing between the ground-state potential $\tilde{E}_{0;0;+}(\mathbf{r})$ and the potential $\tilde{E}_{1;0;+}(\mathbf{r})$ observed at $r=r_C$ for $\vartheta=\pi/2$ in Fig. 13(a) is now clearly visible in transparency, below the upper layer.

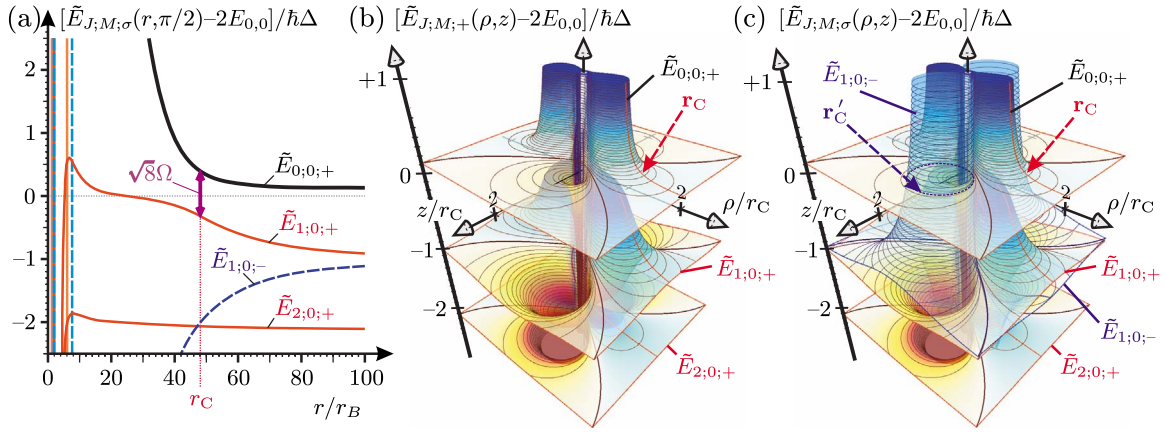


FIG. 13. (Color online) Dressed adiabatic potentials $\tilde{E}_{J;M;\sigma}(\mathbf{r})$ of Eq. (47) for the interaction of two molecules polarized by a (weak) dc field $\mathbf{E}_{dc}=E_{dc}\mathbf{e}_z$ with $\beta\equiv dE_{dc}/B=1/10$ and dressed by an ac field with linear polarization $q=0$. The ac-field detuning and Rabi frequency are $\Delta=3B/10^6\hbar$ and $\Omega=\Delta/4$, respectively. For a typical rotational spacing of $B\sim h\times 10$ GHz these numbers entail $\Delta/2\pi=30$ kHz and $\Omega/2\pi=7.5$ kHz. (a) Dressed adiabatic potentials $\tilde{E}_n(\mathbf{r})$ of Eq. (47) plotted as a function of $r$ for $z=0$ ($\vartheta=\pi/2$). The potentials corresponding to symmetric (antisymmetric) states are given by solid (dashed) lines, and indicated by $\tilde{E}_{J;M;\sigma}(\mathbf{r})$ for $J=0,1,2$, $M=0$, $\sigma=+$ ($J=1$, $M=0$, $\sigma=-$). The dressed ground-state potential $\tilde{E}_{0;0;+}(\mathbf{r})$ has the highest energy (thick solid line). The other potentials are asymptotically detuned by multiples of $\Delta$. The ground-state potential $\tilde{E}_{0;0;+}(\mathbf{r})$ shows an avoided crossing with the symmetric potential $\tilde{E}_{1;0;+}(\mathbf{r})$ at $r=r_C$. (b) Dressed adiabatic potentials $\tilde{E}_{J;M;\sigma}(\mathbf{r})\equiv\tilde{E}_{J;M;\sigma}(\rho,z)$ for the symmetric states ($\sigma=+$) of Eq. (47) plotted as a function of $\rho=r\sin\vartheta$ and $z=r\cos\vartheta$. Darker regions (in the online version: darker red/darker blue) correspond to stronger repulsive/attraction. For $z=0$ ($\rho$ axis) we recognize the case of (a), where the symmetric ground-state potential has the largest energy. The position of the Condon point $r_C$ is indicated by an arrow. Accordingly, the avoided crossing with the potential $\tilde{E}_{1;0;+}(\mathbf{r})$ observed at $r=r_C$ in (a) is now clearly visible in transparency, below the upper layer. For $|z|>0$ the potential $\tilde{E}_{1;0;+}$ becomes less and less repulsive. For $|z|>\rho/\sqrt{2}$ we have $1-3\cos^2\vartheta<0$, and thus $\tilde{E}_{1;0;+}(\mathbf{r})$ is attractive and the Condon point vanishes since the two states are off resonant. (c) Dressed adiabatic potential as in (b), but also showing the antisymmetric states ($\sigma=-$). We see that the dressed potential $\tilde{E}_{1;0;-}(\mathbf{r})$ for the antisymmetric state with $(1;0;-)$ is strongly attractive in the plane, i.e., for $z=0$, which corresponds to the profile shown in (a). With increasingly separation $|z|/r>0$ the potential become less and less attractive. For $|z|/\rho>1/\sqrt{2}$ we have $3\cos^2\vartheta-1>0$ and the potential becomes repulsive. Thereby a crossing between the asymmetric state and the ground state appears at a (second) Condon point $\mathbf{r}'_C$ (dashed line), as the two states are resonant, but due to the permutation symmetry do not couple.

The figure shows that for $|z|>0$ the potential $\tilde{E}_{1;0;+}(\rho,z)$ becomes less and less repulsive, and thus the Condon point $\mathbf{r}_C=r_C(\vartheta)\mathbf{e}_r$ occurs at shorter distances [see below, Eq. (50)]. For $|z|>\rho/\sqrt{2}$, we have $1-3\cos^2\vartheta<0$ and therefore $\tilde{E}_{1;0;+}(\mathbf{r})$ becomes attractive. Thus, the Condon point vanishes since the combined energy of the bare ground state plus a photon and the energy $E_{1;0;+}(\mathbf{r})$ of the bare state $|\Phi_{1;0;+}(\mathbf{r})\rangle$ are not resonant [for the dependence of the bare potential $E_{1;0;+}(\mathbf{r})$ on the angle $\vartheta$, see also Figs. 6(b) and 6(d)]. This vanishing of the avoided crossing for $|z|>\rho/\sqrt{2}$ corresponds to the formation of a hole in the 3D potential shielding the molecular-core region, and it allows for the familiar attraction of dipole-dipole interactions. The presence of this hole is reminiscent of the vanishing of the Condon point at $\vartheta=0$ and $\vartheta=\pi$ for the case of a linearly polarized ac field in the absence of a dc field [see Fig. 11(a2) in Sec. III B]. However, here there are no dark states present at $r_C$, due to the dc-field-induced splitting $\hbar\delta$ of the $J=1$ manifold. This fact eliminates a significant nonadiabatic loss channel for ground-state interactions.

From Fig. 13(b) we see that a real crossing with the antisymmetric state $|\Phi_{1;0;-}(\mathbf{r})\rangle$ takes place for $|z|>\rho/\sqrt{2}$ at a second Condon point, which we denote as $\mathbf{r}'_C$. This is at variance with the case of Sec. III B [see Fig. 11(a1)], where one had $r'_C>r_C$ for all angles, thus opening loss channels due to three-body-induced (or tensor-shift-induced, when a harmonic confinement along $z$ is considered) couplings to the symmetric ground-state for any $\vartheta$. The exact position of the point $\mathbf{r}'_C$ is obtained in the next section.

### 3. Effective 3D interaction potential

In the following we are interested in the effective 3D potential $V_{\text{eff}}^{3D}(\mathbf{r})$ for two molecules in their ground state dressed by the external fields. In the absence of a trap ($\omega_\perp=0$) $V_{\text{eff}}^{3D}(\mathbf{r})$ reads

$$V_{\text{eff}}^{3D}(\mathbf{r})\equiv\tilde{E}_{0;0;+}(r,\vartheta)-2[E_{0,0}+E'_{0,0}], \tag{48}$$

where the terms in brackets are the Stark-shifts $E_{0,0}\approx-d^2\beta^2/6$ and $E'_{0,0}\approx\hbar\Omega^2/\Delta$ induced by the dc and ac electric fields, respectively.

At separations $r\gg r_C$ the effective potential resembles the dipolar potential for two dipoles aligned along $\mathbf{e}_z$ and in second order in the saturation amplitude $\Omega/\Delta$ is given by

$$V_{\rm eff}^{\rm 3D}(\mathbf{r}) \approx \frac{C_{3;(0;0;+)}\Upsilon}{r^3} + \frac{2\Omega^2}{\Delta^2}\frac{(C_{3;(1;0;+)} - C_{3;(0;0;+)})\Upsilon}{r^3}, \tag{49}$$

where $\Upsilon \equiv 1-3\cos^2\vartheta$, and terms of order $O(\Omega^4)$ and $O(1/r^6)$ have been neglected. The first term in Eq. (49) is the dipole-dipole interaction for the two weakly polarized molecules induced by the dc field (see Sec. III A 2), while the second term is the familiar dipole-dipole interaction induced by the coupling to the ac field. The proportionality factor $(C_{3;(1;0;+)}-C_{3;(0;0;+)})2\Omega^2/\Delta^2$ appears due to the competition of the oscillating dipole moment ($\sim d\Omega/\Delta$) induced by the ac field with the permanent dipole moment already present because of the dc field.

The perturbative expression Eq. (49) breaks down when the level spacing becomes comparable to the coupling, that is, for $|\Delta_{1;0}^{(+)}(\mathbf{r}) - \Delta_{0;0}^{(+)}| \sim \Omega$. In particular, for $\Delta_{1;0}^{(+)}(\mathbf{r}_{\rm C}) = \Delta_{0;0}^{(+)}(\mathbf{r}_{\rm C})$ an avoided crossing occurs between the potentials $\tilde{E}_{0;0;+}(\mathbf{r})$ and $\tilde{E}_{1;0;+}(\mathbf{r})$, which defines the resonant Condon point, $\mathbf{r}_{\rm C} \equiv r_{\rm C}(\vartheta)\mathbf{e}_r$, where $\mathbf{e}_r$ is the intermolecular axis. The Condon distance $r_{\rm C}(\vartheta)$ is parametrized in terms of the polar angle $\vartheta$ as

$$r_{\rm C}(\vartheta) = \left(\frac{C_{3;(1;0;+)} - C_{3;(0;0;+)}}{\hbar\Delta(1-3\cos^2\vartheta)}\right)^{1/3}. \tag{50}$$

For $\vartheta = \pi/2$ $(z/r=0)$ the Condon point is attained at $r_{\rm C} = r_{\rm C}(\pi/2) = [(C_{3;(1;0;+)} - C_{3;(0;0;+)})/\hbar\Delta]^{1/3} \approx [d^2/3\hbar\Delta]^{1/3}$ [see Fig. 12(a)], which depends on the detuning $\Delta$ and the difference in the $C_{3;n}$ coefficients of the first excited state and the ground state $(C_{3;(1;0;+)} - C_{3;(0;0;+)} \approx d^2/3$ for a weak dc field $\beta \ll 1)$. For $\vartheta \neq \pi/2$ $(z/r \neq 0)$ the avoided crossing occurs at smaller separations $r_{\rm C}(\vartheta) < r_{\rm C}$ until it vanishes for $\cos^2\vartheta = (z/r)^2 = 1/3$ [see Fig. 12(b)].

The position of the point $\mathbf{r}'_{\rm C} \equiv r'_{\rm C}(\vartheta)\mathbf{e}_r$ is determined by the crossing between the dressed ground-state potential $\tilde{E}_{0;0;+}(\mathbf{r})$ and the potential for the antisymmetric state, $\tilde{E}_{1;0;-}(\mathbf{r})$. As mentioned above [and shown in Fig. 13(b)], this crossing occurs in the region $|z| > \rho/2$ $(\cos^2\vartheta > 1/3)$. The distance $r'_{\rm C}(\vartheta)$ is given by $r'_{\rm C}(\vartheta) \approx [(C_{3;(0;0;+)} - C_{3;(1;0;-)}) \times (3\cos^2\vartheta - 1)/\hbar\Delta]^{1/3}$.

The discussion above suggests that an effective 2D interaction potential $V_{\rm eff}^{\rm 2D}(\boldsymbol{\rho})$ with no losses due to couplings of the ground state to other symmetric or antisymmetric states may be obtained for distances $r \gg r_\delta$, by introducing a parabolic potential in the $z$ direction confining the particles to the sector $(z/r)^2 < 1/3$. This shielding of the loss channels is analogous to the shielding of the attractive part of the potential and of the molecular-core region of the dc case for $r > \ell_\perp \gg r_\star \sim (d^2/B\beta^2)^{1/3}$ (see Sec. III A). However, now $\ell_\perp$ is effectively replaced by $r_{\rm C} \gtrsim \ell_\perp$, and $r_{\rm C}$ allows for much greater flexibility in tuning by external fields.

In the next section we detail the requirements for obtaining a stable effective interaction in 2D. In this way, it is possible to realize the 2D potential with steplike character, as shown in Fig. 2.

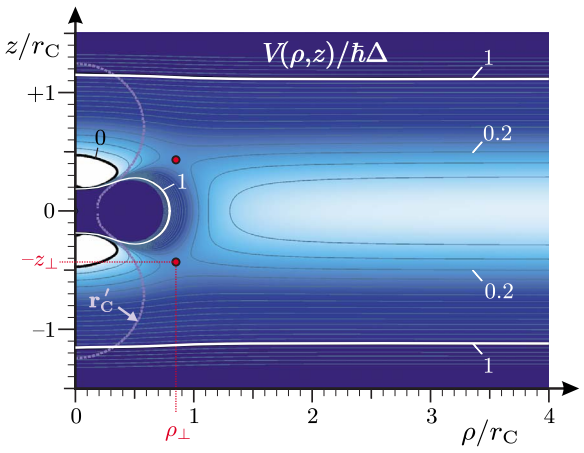


FIG. 14. (Color online) Contour plot of the effective potential $V(\rho,z)$ of Eq. (51) for two polar molecules interacting in the presence of a weak dc field and an ac field. The field parameters are the same as in Fig. 13. The frequency of the confining harmonic potential in the $z$ direction is $\omega_\perp = \Delta/5$. Darker regions represent stronger repulsive interactions. The white region for $\rho < 1/2$ indicates a potential $V(\rho,z) < 0$. The combination of the dipole-dipole interactions induced by the dc electric and ac (microwave) fields and of the quadratic confinement leads to realization of a 3D repulsive potential for $r \gg r_{\rm C}$. In particular, two saddle points located at $(\rho_\perp, \pm z_\perp)$ (circles) separate the repulsive long-distance regime $r \gg r_{\rm C}$ from the short-distance regime $r < r_{\rm C}$ where diabatic losses occur. The dotted line signaled by $\mathbf{r}'_{\rm C}$ indicates the location of the crossing between the ground-state potential and the energy $\tilde{E}_{1;0;-1}(\mathbf{r})$ of the antisymmetric state (see text and Fig. 13).

#### *4. Parabolic confinement*

The presence of a finite trapping potential of frequency $\omega_\perp$ in the $z$ direction provides for a position-dependent energy shift of Eq. (49). Thus, the new potential reads

$$V(\rho,z) \equiv V_{\rm eff}^{\rm 3D}(\mathbf{r}) + \frac{1}{4}m\omega_\perp^2 z^2. \tag{51}$$

Analogously to the discussion of Sec. III A 3, the combination of the dipole-dipole interaction, which is repulsive for $r \gg r_{\rm C}$, and of the harmonic confinement yields a repulsive potential which provides for a three-dimensional barrier separating the long-distance repulsive regime from the short-distance regime, where collisional losses can occur. If the collisional energy is much smaller than this barrier, the relative motion of the particles is confined to the long-distance region, where the potential is purely repulsive.

Figure 14 is a contour plot of Eq. (51) for the same parameters as in Fig. 13, i.e., $\Delta = 4\Omega = 3B/10^6\hbar$ and $\beta = 1/10$. The frequency $\omega_\perp$ for the harmonic confinement is $\omega_\perp = \Delta/5$. In the figure, darker regions correspond to a stronger repulsive potential, and the white region for $\rho, z \lesssim r_{\rm C}/2$ corresponds to $V(\rho,z) < 0$. The repulsion due to the dipole-dipole and harmonic potentials is clearly distinguishable at $z=0$ and $|z|/r_{\rm C} \gtrsim 1$, respectively. Two saddle points located at $(\rho_\perp, \pm z_\perp)$ separate the repulsive long-distance from the short-distance regions (circles in Fig. 14). The location of the saddle points approaches $(\rho_\perp, |z_\perp|) \sim (r_{\rm C}, r_{\rm C}/2)$ with increas-

ing confining potential $\omega_\perp$ in the $z$ direction. In the figure, the dotted line signaled by $\mathbf{r}'_C$ marks the location of the crossing between the dressed ground-state potential $\tilde{E}_{0;0;+}(\mathbf{r})$ and the potential $\tilde{E}_{1;0;-}(\mathbf{r})$ for the antisymmetric state. The figure shows that this crossing occurs in the short-distance region $r<r_C$ for all $z$, in agreement with previous discussions. Thus, for $r \gg r_C$ and collisional kinetic energies smaller than the potential barrier at the saddle point the ground-state interactions are stable and purely repulsive, consistent with the discussion above.

#### 5. Effective 2D interaction

Analogously to the discussion for the dc-field case in Sec. III A 5, in the limit of tight optical confinement it is possible to derive effective two-dimensional ground interaction potentials $V^{2D}_{\rm eff}(\boldsymbol{\rho})$ by integrating over the fast transverse degrees of freedom, $z_1$ and $z_2$. For $r>r_C \gg a_\perp$, the two-particle eigenfunctions in the $z$ direction approximately factorize into products of single-particle harmonic oscillator wave functions, and thus the integration is conveniently carried out in the harmonic oscillator basis. In the adiabatic approximation we find to first order in $V^{3D}_{\rm eff}(\mathbf{r})/\hbar\omega_\perp$ the 2D effective ground-state potential as

$$V^{2D}_{\rm eff}(\boldsymbol{\rho}) \approx \int dz_1 dz_2 |\psi_0(z_1)|^2 |\psi_0(z_2)|^2 V^{3D}_{\rm eff}(\boldsymbol{\rho}, z_2 - z_1)$$

$$= \frac{1}{\sqrt{2\pi} a_\perp} \int dz\, e^{-z^2/2a_\perp^2} V^{3D}_{\rm eff}(\rho, z), \qquad (52)$$

where $\psi_k(z_j)$ is the $k$th harmonic oscillator wave function for the transverse confinement. In an analogous way, effective 2D potentials can be derived for all the dressed potentials $\tilde{E}_{J;M;\sigma}(\mathbf{r})$, as (up to a constant shift)

$$\tilde{E}^{2D}_{J;M;\sigma}(\boldsymbol{\rho}) \approx \frac{1}{\sqrt{2\pi} a_\perp} \int dz\, e^{-z^2/2a_\perp^2} \tilde{E}_{J;M;\sigma}(\rho, z), \qquad (53)$$

with $\tilde{E}^{2D}_{0;0;+}(\boldsymbol{\rho}) = V^{2D}_{\rm eff}(\boldsymbol{\rho})$. In the following we discuss the validity of the adiabatic approximation in the case when both dc and the ac fields are present. We focus only on the four above-mentioned potentials, since the remaining states of the $J=1$ manifold are detuned by a large amount $\sim \delta/\omega_\perp \sim 10^3$. Thus, we neglect nonadiabatic couplings from the ground state to the continuum corresponding to high-energy transverse excitations of the far-detuned states, since these couplings are expected to vanish at large interparticle separations.

At variance with the dc-field case of Sec. III A 5, satisfying the adiabatic approximation in the presence of both dc and ac fields is nontrivial. In fact, for a blue-detuned ($\Delta>0$) ac field the dressed ground-state potential $\tilde{E}_{0;0;+}(\mathbf{r})$ has the largest energy [see Fig. 13(a)]. Thus, it can happen that $\tilde{E}_{0;0;+}(\mathbf{r})$ becomes degenerate with the energy of one of the other states plus some multiple $k$ of the harmonic oscillator energy in the transverse direction $\hbar\omega_\perp$. When these degeneracies happen, avoided and real crossings occur with the energies of the symmetric and the antisymmetric states, so that satisfying the adiabatic requirement becomes in general much harder than in the dc-field case of Sec. III A 5. In fact, there the ground state is the lowest-energy state and the lowest-energy excitations are those of the harmonic oscillator along $z$. In that case the adiabaticity condition is satisfied for $V^{2D}_{\rm eff}(\boldsymbol{\rho}) \ll \hbar\omega_\perp$. On the other hand, it is still possible to derive an expression analogous to the latter even for the case when the ac field is present, if the trapping potential is large enough so that $\omega_\perp \gtrsim 2\Delta$. In fact, then for large distances $\rho \gg r_C$ the energy difference between $\tilde{E}_{0;0;+}(\mathbf{r})$ and that of the first excited state is approximately $\hbar\omega_\perp - 2\hbar\Delta$, where $-2\hbar\Delta$ is the energy $\tilde{E}_{2;0;+}(\mathbf{r}) = -2\hbar\Delta$ (see Fig. 13). In this case, the adiabatic approximation is still valid provided

$$V^{2D}_{\rm eff}(\rho) \ll \hbar\omega_\perp - 2\hbar\Delta. \qquad (54)$$

The perturbative expressions Eq. (53) for the dressed effective 2D potentials $\tilde{E}^{2D}_{J;0;\sigma}(\boldsymbol{\rho})$ are shown as thick dashed lines in Fig. 15 for the combination of a weak dc field with $\beta = 1/10$ and an ac field with linear polarization $q=0$ and detuning $\Delta = 4\Omega = 3B/10^6\hbar$. Figures 15(a)–15(c) represent different transverse trapping frequencies given by $\omega_\perp/\Delta = 1/2, 2, 5$, respectively. The effective potential for the ground state, $\tilde{E}^{2D}_{0;0;+}$, is indicated at large separation $\rho \gg r_C$, where it approaches the value $\tilde{E}^{2D}_{0;0;+}(\rho\to\infty) = 2E_{0,0} + 2E'_{0,0}$, corresponding to the dc and ac Stark shift of the separated molecules, with $2E'_{0,0}/\hbar\Delta \approx +2(\Omega/\Delta)^2 = 1/8$. The thin solid and dotted lines in Fig. 15 show the potentials $\tilde{E}^{2D}_{J;M;\sigma;k}(\boldsymbol{\rho})$ for $\sigma=+$ and $\sigma=-$, respectively. The potentials $\tilde{E}^{2D}_{J;M;\sigma;k}(\boldsymbol{\rho})$ have been obtained by diagonalizing numerically

$$\tilde{H}_{\rm rel} = \frac{p_z^2}{m} + \frac{1}{4} m\omega_\perp^2 z^2 - \frac{\hbar\omega_\perp}{2} + \tilde{H}_{\rm int}(\mathbf{r}), \qquad (55)$$

with $\tilde{H}_{\rm int}(\mathbf{r})$ given in Eq. (46). Here, the index $k=0,1,2,\ldots$ labels the transverse excitations and at large separations $\rho \gg r_C$ the corresponding potentials approach

$$\tilde{E}^{2D}_{J;M;\sigma;k}(\rho \to \infty) \approx \tilde{E}_{J;M;\sigma}(r \to \infty) + k\hbar\omega_\perp.$$

In Fig. 15(a) we observe a series of avoided crossings involving the ground-state potential in the region $\rho \lesssim r_C$. For $\rho \gg r_C$ the ground-state potential has the characteristic $1/\rho^3$ dependence. Figure 15(b) shows that for $\omega_\perp = 2\Delta$ the ground-state potential $V^{2D}_{\rm eff}(\boldsymbol{\rho})$ is already well separated from the energy of the first excited state with $k>0$ in a region $\rho > r_C$. Finally, Fig. 15(c) shows that for a tight trapping, $\omega_\perp = 5\Delta$, the ground-state potential $V^{2D}_{\rm eff}(\boldsymbol{\rho})$ for $\rho > r_C/2$ is well separated by $\hbar\Delta$ from all the excited states with $k>0$. The adiabatic approximation is valid for $V^{2D}_{\rm eff}(\boldsymbol{\rho}) \ll \hbar\Delta$, consistent with Eq. (54).

Remarkably, we find that, since the spontaneous emission rates in the excited rotational levels of polar molecules, $\Gamma_{\rm SE}$, are negligible compared to achievable optical confinements $\sim\omega_\perp \sim 2\pi \times 150$ kHz, the regime where $\Delta < \omega_\perp/2$ is widely accessible. In fact one can achieve the limit of weak saturation and strong confinement with at the same time sufficient detuning to avoid spontaneous emission. That is, it is possible to satisfy all of the inequalities $\Gamma_{\rm SE} \ll \Omega < 2\Delta < \omega_\perp$.

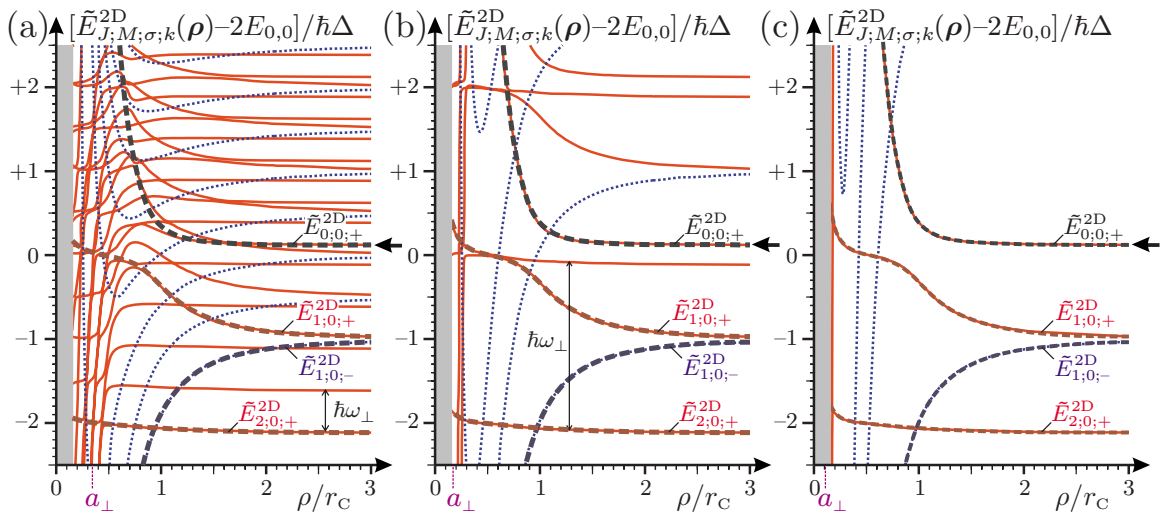


FIG. 15. (Color online) Effective 2D potentials $\tilde{E}^{2D}_{J;M;\sigma;k}(\boldsymbol{\rho})$ with $(J=0,1,2;M=0;\sigma=\pm1;k=0,1,2,\ldots)$ of Eq. (55) for the ac- and dc-field setups of Fig. 14. The strength of the (weak) dc field is $\beta=dE_{dc}/B=1/10$. The ac field has polarization $q=0$, is blue detuned by $\Delta=3B/10^6\hbar$, and the saturation amplitude is $\Omega/\Delta=1/4$. (a), (b), and (c) correspond to a harmonic oscillator frequency of the confining potential $\omega_\perp/\Delta=1/2,2$, and 5, respectively. The thick dashed lines indicate the (single-band) effective potentials $\tilde{E}^{2D}_{J;0;\sigma}(\boldsymbol{\rho})$ of Eq. (53). The solid lines are the nonperturbative potentials $E^{2D}_{J;0;\sigma;k}(\boldsymbol{\rho})$ of Eq. (55), where $k=0,1,2,\ldots$ denote the $k$th transversal excitations in the $z$ direction. The ground-state potential approaches twice the single-particle Stark shifts, $2(E_{0;0}+E'_{0;0})$ (see text), for $\rho\to\infty$ and it is indicated by arrow(s). The harmonic oscillator length $a_\perp$ for a typical mass $m\approx100$ amu, a dipole moment $d\approx8.9$ D, and a rotational constant $B\approx h\times10$ GHz is indicated on the $\rho$ axis. The corresponding detuning is $\Delta\approx2\pi\times30$ kHz and the trapping frequency is $\omega_\perp/2\pi\approx15$, 60, and 150 kHz in (a), (b), and (c), respectively. The gray region corresponds to $r<r_\delta$.

## IV. CONCLUSIONS

In this work, we have shown how to engineer 2D interaction potentials for optically trapped polar molecules in their electronic and vibrational ground state. In particular, we have shown how to modify the shape as well as the strength of the interparticle interaction potentials, by manipulating the rotational dynamics using external dc and ac microwave fields in combination with dipole-dipole interactions. In Sec. III A we have shown that in the presence of a dc field and of a tight optical confinement it is possible to realize effective 2D potentials, where particles interact via a purely repulsive $\sim1/r^3$ interaction. A potential barrier shields the attractive inner region of the interaction potential, thus providing for the stability of the collisional setup. In Sec. III B we analyzed the interactions in the presence of an ac field. We derived the 3D adiabatic potentials for the molecular interactions, finding several degeneracies in the two-particle spectrum at distances of the order of the resonant Condon point $r_C$ between the energy of the ground state plus one photon and states of the first excited manifold. The presence of these degeneracies opens (diabatic, three-body-induced, and, for the case of transverse confinement, residual tensor-shift-induced) loss channels for the ground-state collisions, which make the case of interactions in a pure ac field less appealing for realizing stable collisional setups in two dimensions. In Sec. III C we showed that it is possible to realize stable 2D interaction setups with considerable flexibility in potential design by combining dc and ac fields, in the presence of strong transverse confinement. In fact, the dc field helps to greatly suppress the presence of loss channels at large distances, while the ac field allows for realizing potentials whose shape can vary markedly between the long- and short-distance regimes.

## ACKNOWLEDGMENTS

The authors thank Roman V. Krems and Paul S. Julienne for stimulating and helpful discussions. This work was supported by the Austrian Science Foundation (FWF), the European Union projects OLAQUI (Grant No. FP6-013501-OLAQUI) and CONQUEST (Grant No. MRTN-CT-2003-505089), the SCALA network (IST-15714) and the Institute for Quantum Information.

[1] For an overview, see, e.g., Ultracold matter, edited by K. Southwell, special issue of Nature (London) **416**, 205 (2002).

[2] See, e.g., Ultracold Polar Molecules: Formation and Collisions, edited by J. Doyle, B. Friedrich, R. V. Krems, and F. Masnou-Seeuws, special issue of Eur. Phys. J. D **31**, 149 (2004).

[3] J. M. Sage, S. Sainis, T. Bergeman, and D. DeMille, Phys. Rev. Lett. **94**, 203001 (2005).

[4] H. L. Bethlem, G. Berden, F. M. H. Crompvoets, R. T. Jongma, A. J. A. van Roij, and G. Meijer, Nature (London)

**406**, 491 (2000).
[5] J. D. Weinstein, R. deCarvalho, T. Guillet, B. Friedrich, and J. M. Doyle, Nature (London) **395**, 148 (1998).
[6] F. M. H. Crompvoets, H. L. Bethlem, R. T. Jongma, and G. Meijer, Nature (London) **411**, 174 (2001).
[7] T. Junglen, T. Rieger, S. A. Rangwala, P. W. H. Pinkse, and G. Rempe, Phys. Rev. Lett. **92**, 223001 (2004).
[8] M. R. Tarbutt, H. L. Bethlem, J. J. Hudson, V. L. Ryabov, V. A. Ryzhov, B. E. Sauer, G. Meijer, and E. A. Hinds, Phys. Rev. Lett. **92**, 173002 (2004).
[9] M. W. Mancini, G. D. Telles, A. R. L. Caires, V. S. Bagnato, and L. G. Marcassa, Phys. Rev. Lett. **92**, 133203 (2004).
[10] T. Rieger, T. Junglen, S. A. Rangwala, P. W. H. Pinkse, and G. Rempe, Phys. Rev. Lett. **95**, 173002 (2005).
[11] D. Wang, J. Qi, M. F. Stone, O. Nikolayeva, H. Wang, B. Hattaway, S. D. Gensemer, P. L. Gould, E. E. Eyler, and W. C. Stwalley, Phys. Rev. Lett. **93**, 243005 (2004).
[12] S. Y. T. van de Meerakker, P. H. M. Smeets, N. Vanhaecke, R. T. Jongma, and G. Meijer, Phys. Rev. Lett. **94**, 023004 (2005).
[13] S. D. Kraft, P. Staanum, J. Lange, L. Vogel, R. Wester, and M. Weidemüller, J. Phys. B **39**, S993 (2006).
[14] B. C. Sawyer, B. L. Lev, E. R. Hudson, B. K. Stuhl, M. Lara, J. L. Bohn, and Jun Ye, Phys. Rev. Lett. **98**, 253002 (2007).
[15] W. C. Stwalley, Eur. Phys. J. D **31**, 221 (2004).
[16] E. R. Hudson, J. R. Bochinski, H. J. Lewandowski, B. C. Sawyer, and J. Ye, Eur. Phys. J. D **31**, 351 (2004).
[17] S. Inouye, J. Goldwin, M. L. Olsen, C. Ticknor, J. L. Bohn, and D. S. Jin, Phys. Rev. Lett. **93**, 183201 (2004).
[18] D. DeMille, Phys. Rev. Lett. **88**, 067901 (2002).
[19] M. Greiner, C. A. Regal, and D. S. Jin, Nature (London) **426**, 537 (2003).
[20] C. A. Regal, C. Ticknor, J. L. Bohn, and D. S. Jin, Nature (London) **424**, 47 (2003).
[21] T. Volz, N. Syassen, D. M. Bauer, E. Hansis, S. Dürr, and G. Rempe, Nat. Phys. **2**, 692 (2006).
[22] A. Micheli, G. K. Brennen, and P. Zoller, Nat. Phys. **2**, 341 (2006).
[23] U. Fano, Phys. Rev. **124**, 1866 (1961).
[24] For a review on Feshbach resonances, see, e.g., R. A. Duine and H. T. C. Stoof, Phys. Rep. **396**, 115 (2004).
[25] M. Greiner, O. Mandel, T. Esslinger, T. W. Hänsch, and I. Bloch, Nature (London) **415**, 39 (2002).
[26] C. A. Regal, M. Greiner, and D. S. Jin, Phys. Rev. Lett. **92**, 040403 (2004).
[27] M. Bartenstein, A. Altmeyer, S. Riedl, S. Jochim, C. Chin, J. H. Denschlag, and R. Grimm, Phys. Rev. Lett. **92**, 120401 (2004).
[28] M. W. Zwierlein, J. R. Abo-Shaeer, A. Schirotzek, C. H. Schunck, and W. Ketterle, Nature (London) **435**, 1047 (2005).
[29] G. B. Partridge, K. E. Strecker, R. I. Kamar, M. W. Jack, and R. G. Hulet, Phys. Rev. Lett. **95**, 020404 (2005).
[30] C. Chin, M. Bartenstein, A. Altmeyer, S. Riedl, S. Jochim, J. Hecker Denschlag, and R. Grimm, Science **305**, 1128 (2005).
[31] H. P. Büchler, E. Demler, M. D. Lukin, A. Micheli, N. V. Prokof'ev, G. Pupillo, and P. Zoller, Phys. Rev. Lett. **98**, 060404 (2007).
[32] R. V. Krems, Int. Rev. Phys. Chem. **24**, 99 (2005).
[33] R. V. Krems, Phys. Rev. Lett. **96**, 123202 (2006).
[34] A. V. Avdeenkov and J. L. Bohn, Phys. Rev. Lett. **90**, 043006 (2003).
[35] C. Ticknor and J. L. Bohn, Phys. Rev. A **72**, 032717 (2005).
[36] G. E. Astrakharchik, J. Boronat, I. L. Kurbakov, and Yu. E. Lozovik, Phys. Rev. Lett. **98**, 060405 (2007).
[37] R. K. Kalia and P. Vashishta, J. Phys. C **14**, L643 (1981).
[38] V. L. Berezinskii, Sov. Phys. JETP **34**, 610 (1972).
[39] J. M. Kosterlitz and D. J. Thouless, J. Phys. C **6**, 1181 (1973).
[40] R. Napolitano, J. Weiner, and P. S. Julienne, Phys. Rev. A **55**, 1191 (1997).
[41] J. Weiner, V. S. Bagnato and S. Zilio, and P. S. Julienne, Rev. Mod. Phys. **71**, 1 (1999).
[42] S. C. Zilio, L. Marcassa, S. Muniz, R. Horowicz, V. Bagnato, R. Napolitano, J. Weiner, and P. S. Julienne, Phys. Rev. Lett. **76**, 2033 (1996).
[43] G. Herzberg, *Molecular Spectra and Molecular Structure I: Spectra of Diatomic Molecules* (Van Nostrand Reinhold, New York, 1950).
[44] J. M. Brown and A. Carrington, *Rotational Spectroscopy of Diatomic Molecules* (Cambridge University Press, New York, 2003).
[45] B. R. Judd, *Angular Momentum Theory for Diatomic Molecules* (Academic Press, New York, 1975).
[46] See, e.g., http://physics.nist.gov/PhysRefData/MolSpec/Diatomic
[47] See, e.g., C. H. Townes and A. L. Shawlow, *Microwave Spectroscopy* (McGraw-Hill, New York, 1955).
[48] S. Kotochigova and E. Tiesinga, Phys. Rev. A **73**, 041405(R) (2006).
[49] B. Friedrich and D. Herschbach, Phys. Rev. Lett. **74**, 4623 (1995).
[50] D. C. E. Bortolotti, S. Ronen, J. L. Bohn, and D. Blume, Phys. Rev. Lett. **97**, 160402 (2006).
[51] See also L. Santos, G. V. Shlyapnikov, and M. Lewenstein, Phys. Rev. Lett. **90**, 250403 (2003).
[52] S. Coleman, Phys. Rev. D **15**, 2929 (1977).